CHAPTER 10

FREQUENCY - SHAPED LARGE - ANGLE MANEUVERS OF FLEXIBLE SPACECRAFT

10.1 INTRODUCTION

In this chapter we consider the problem of maneuvering a flexible vehicle through large rigid body motions about a principal axis, while using derivative penalty performance indices for smoothing the resulting control torque profiles. These results extend significantly the developments of Chapter 9. In particular, we consider the class of maneuvers in which several actuators are simultaneously employed, and the plant dynamics is modelled as being linear and time-invariant. As in Chapter 9 we impose the constraint of zero flexural deformations and deformation rates at the terminal maneuver time. However, as shown in Section 10.4.3 additional constraints can be constructively imposed on both the controls and the elastic deformations for special classes of slewing maneuvers.

The frequency-shaped control design technique described in this chapter is achieved by using standard time domain techniques, whereby quadratic penalties on the first- and higher-order time derivatives of the control are introduced into the performance index, as done in Chapter 6. Inclusion of control-rate penalties into the performance index accomplishes two qualitatively important objectives. First, the terminal on/off jump discontinuities in the control time history can be moved into the higher control time derivatives, thus dramatically reducing the high frequency content of the applied control. As a result, the control-rate penalties act like control-smoothing penalties, since the implemented control is free of terminal discontinuities through several time derivatives of the control. An additional important benefit of employing frequency-shaped techniques is that the high frequency content of the applied control rolls off very rapidly; thus the problem of potentially destabilizing control spillover effects for unmodeled high frequency structural dynamics is

greatly reduced. Nevertheless, it remains the responsibility of the analyst to select a suitable reduced-order model for any control application, in order to minimize the potential destabilizing affects of control spillover. In a qualitative sense, the spillover problem can be investigated by evaluating the control influence on a suitable residual plant model, as shown in Section 10.4.7.

Second, the use of control-rate penalties permits the control designer to directly specify constraints which govern the terminal values of the control and various time derivatives of the control. For example in rest-to-rest maneuvers, it is convenient to specify that the control system is turned off both intially and finally. Of course, depending on the particular mission objectives (as shown in the combined slew and terminal target tracking maneuver of Section 10.4.3), other physically meaningful kinematical boundary conditions for the terminal control and control-rates can be specified.

A number of authors have considered various techniques for generating frequency-shaped control designs for maneuvering flexible spacecraft (refs. 1-10). The derivative penalty ideas presented in this chapter were first introduced by Moore and Anderson in ref. 15. Recent extentions by Gupta et al. in refs. 12-14 permit significant generalizations of the derivative penalty approach, however these generalizations are not considered here.

The specific model considered in this chapter (Figures 10.1 and 10.2) consists of a rigid hub with four identical elastic appendages attached symmetrically about the central hub. In particular, we consider the following idealizations: (i) single-axis maneuvers; (ii) in-plane motion; (iii) anti-symmetric deformations; (iv) small linear flexural deformations; (v) only the linear time-invariant form of the equations of motion are considered; and (vi) the control actuators are modelled as concentrated torque generating devices. The multiple actuator control system for the vehicle consists of a single

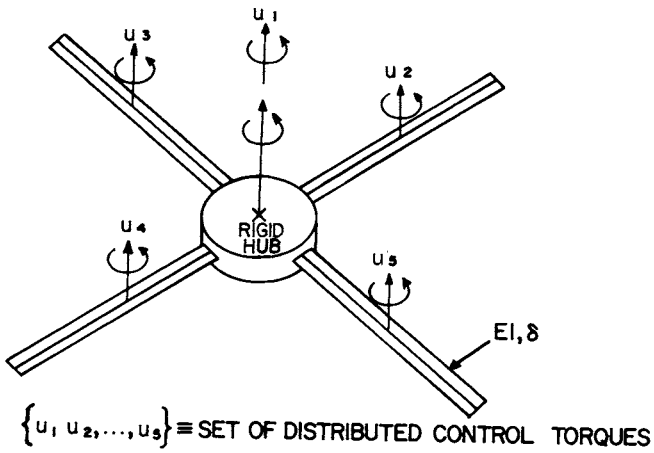

Figure 10.1 Undeformed Configuration

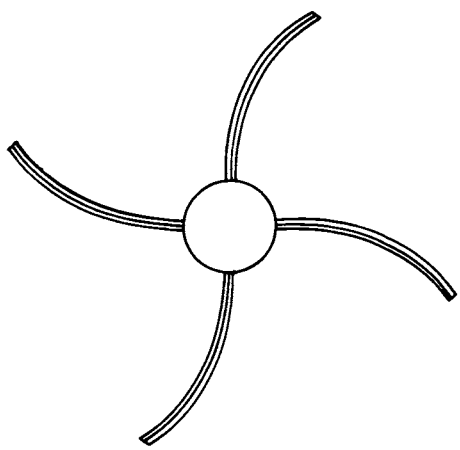

Figure 10.2 Antisymmetric Deformation

controller in the rigid part of the structure, and each elastic appendage is assumed to have an arbitrary number of uniformly spaced discrete controllers along its span. Moreover, in the optimal control performance index, the control weighting matrices are adjusted in order to have the rigid body control provide the primary torque for maneuvering the vehicle, while the appendage actuators act principally as vibration suppressors.

In Section 10.2, the equation of motion is presented for the linear time-invariant problem. The state space form of the equation of motion is given in Section 10.3. The necessary conditions and solution for the control-rate penalty method are presented in Section 10.4. Also presented in Section 10.4 are the necessary extensions for treating combined slew and tracking maneuvers, as well as free final angle maneuvers. Example maneuvers are presented in Section 10.5.

10.2 EQUATION OF MOTION

For the vehicle of Figure 10.1, the linear time-invariant matrix form of the equation of motion can be shown to be (see Eqs. 9.1 through 9.15).

$$M\ddot{\xi} + K\xi = Pu \tag{10.1}$$

where

$$\xi = \begin{Bmatrix} \theta \\ \eta \end{Bmatrix} \; ; \quad M = \begin{bmatrix} \hat{I} & M_{\theta\eta}^T \\ M_{\theta\eta} & M_{\eta\eta} \end{bmatrix} \; ; \quad K = \begin{bmatrix} 0 & 0^T \\ 0 & K_{\eta\eta} \end{bmatrix}$$

$$P = \begin{bmatrix} 1 & 4\nu^T \\ 0 & F \end{bmatrix} \; ; \quad u = \begin{Bmatrix} u_R \\ u_E \end{Bmatrix} \; ; \quad \nu = \begin{Bmatrix} 1 \\ 1 \\ \vdots \\ 1 \end{Bmatrix}, \; (N_{ac} \times 1)$$

$$F = 4 \begin{bmatrix} \phi_1'(x_1 - r) & \phi_1'(x_2 - r) & \cdots & \phi_1'(x_{N_{ac}} - r) \\ \phi_2'(x_1 - r) & \phi_2'(x_2 - r) & \cdots & \phi_2'(x_{N_{ac}} - r) \\ \vdots & \vdots & & \vdots \\ \phi_n'(x_1 - r) & \phi_n'(x_2 - r) & \cdots & \phi_n'(x_{N_{ac}} - r) \end{bmatrix}, \; (n \times N_{ac})$$

where $\theta(t)$ denotes the rigid body rotation angle, $\eta(t)$ denotes the n x 1 vector of time-varying generalized coordinates for the flexible body response, $\hat{I}$ denotes moment of inertia for the undeformed vehicle, $u_R(t)$ denotes the rigid hub control torque, $u_E(t)$ denotes the N_{ac} x 1 vector of control torques acting on each elastic appendage, $x_1, x_2, \ldots, x_{N_{ac}}$ denote the points of application of the actuators along each appendage, $M = M^T > 0$, $K = K^T \geq 0$, P is the control influence matrix, and the integral definitions for $\mathbf{M}_{\theta\eta}$, $M_{\eta\eta}$, and $K_{\eta\eta}$ are given by

$$[\mathbf{M}_{\theta\eta}]_k = 4 \int_r^{r+L} x\, \phi_k(x - r)dm \quad , \quad (n \times 1)$$

$$[M_{\eta\eta}]_{kp} = 4 \int_r^{r+L} \phi_k(x - r)\ \phi_p(x - r)dm \quad , \quad (n \times n)$$

$$[K_{\eta\eta}]_{kp} = 4 \int_r^{r+L} EI\, \phi_k''(x - r)\phi_p''(x - r)dx \quad , \quad (n \times n)$$

$$(\cdot)'' = \frac{d^2}{dx^2}(\cdot)$$

10.3 STATE SPACE FORMULATION

Equation 10.1 is cast into diagonal form by introducing the modal coordinate transformation

$$\xi(t) = Es_1(t) \quad , \quad \dot{\xi}(t) = E\dot{s}_1(t) \quad , \quad E^TME = \Delta \quad , \quad E^TKE = I$$

where E is the normalized eigenvector matrix for the M and K matrices, and Δ is a diagonal matrix containing the squares of the system natural frequencies (eigenvalues). Introducing the transformation above into Eq. 10.1, and premultiplying the resulting equation by E^T, the modal space equation of motion follows as:

$$\ddot{s}_1 + \Delta s_1 = Du \quad ; \quad D = E^TP$$

The equation above can be cast into state space form by introducing the transformation $\dot{s}_1(t) = s_2(t)$, leading to

$$\dot{s} = As + Bu \tag{10.2}$$

where

$$A = \begin{bmatrix} 0 & I \\ -\Delta & 0 \end{bmatrix} , \quad B = \begin{Bmatrix} 0 \\ D \end{Bmatrix} , \quad s = \begin{Bmatrix} s_1 \\ s_2 \end{Bmatrix}$$

10.4 OPTIMAL CONTROL PROBLEM USING THE CONTROL-RATE PENALTY TECHNIQUE

10.4.1 Statement of the Problem

We consider here the rotational dynamics of a flexible space vehicle restricted to a single-axis large-angle maneuver about a principal axis, where the system dynamics is governed by Eq. 10.2. Since the kth time derivative of the control is assumed to be penalized in the performance index, it is convenient to introduce the following augmented state differential equation (ref. 15)

$$\dot{\zeta} = \bar{A}\zeta + \bar{B}u_k \tag{10.3}$$

where

$$\zeta(t) = [s(t), u_0(t), u_1(t), \ldots, u_{k-1}(t)]^T , \quad ((2N + kN_c) \times 1)$$

$$u_0(t) = u(t) , \quad u_r(t) = \frac{d^r u(t)}{dt^r} , \quad r = 1, \ldots, k \quad (k \geq 1)$$

$$\bar{A} = \begin{bmatrix} A & B & 0 \\ 0 & 0 & I \\ 0 & 0 & 0 \end{bmatrix} \begin{matrix} \} \ 2N \\ \} \ (k-1)N_c \\ \} \ N_c \end{matrix}$$

$$\qquad\quad 2N \quad N_c \quad (k-1)N_c$$

$$\bar{B} = \begin{bmatrix} 0 \\ 0 \\ I \end{bmatrix} \begin{matrix} \} \ 2N \\ \} \ (k-1)N_c \\ \} \ N_c \end{matrix}$$

$$\qquad\quad N_c$$

$N_c = N_{ac} + 1$ and $N = n + 1$.

The optimal control problem is then to seek the solution of Eq. (10.3) satisfying the prescribed conditions for $\zeta(t_o)$ and $\zeta(t_f)$, which minimizes the performance index

$$J = \frac{1}{2}\int_{t_o}^{t_f} [\zeta^T Q\zeta + \mathbf{u}_k^T R\mathbf{u}_k]dt \tag{10.4}$$

where $Q = Q^T > 0$ is augmented state weight matrix, and $R = R^T \geq 0$ is the control-rate penalty weight matrix for $\mathbf{u}_k(t)$. As shown by Moore and Anderson (ref. 15) the controllability condition for the pair $(\bar{A}, \bar{B})$ reduces to controllability requirement for the pair (A, B). When k = 0 the results above reduce to the special case considered in Chapter 9. With k > 0 the performance index penalizes the states, controls, and time derivatives of the control; and the resulting control time histories are *smooth* through several time derivatives. Moreover, as shown in the example maneuvers of Section 10.5 the flexible body response is significantly reduced at the terminal maneuver time when the derivative penalty method is used.

10.4.2 Derivation of Necessary Conditions from Pontryagin's Principle

In preparing to make use of Pontryagin's necessary conditions, we introduce the Hamiltonian functional

$$H = \frac{1}{2}(\zeta^T Q\zeta + \mathbf{u}_k^T R\mathbf{u}_k) + \lambda^T(\bar{A}\zeta + \bar{B}\mathbf{u}_k) \tag{10.5}$$

where $\lambda(t)$ is a vector of $2N + kN_c$ Lagrange multipliers. We observe that the form of Eqs. 10.5 and 9.26 are identical, where $\mathbf{s}(t)$ and $\mathbf{u}(t)$ are replaced by $\zeta(t)$ and $\mathbf{u}_k(t)$, respectively. As a result, from Eq. 9.30 it follows that the state and co-state differential equations can be written as

State Equations

$$\dot{\zeta} = \bar{A}\zeta - \bar{B}R^{-1}\bar{B}^T\lambda \tag{10.6a}$$

Co-State Equations

$$\dot{\lambda} = -Q\zeta - \bar{A}^T\lambda \tag{10.6b}$$

10.4.3 Solution for the Initial Co-states

In Eq. 10.6 we observe that the boundary conditions for $\zeta(t)$ are specified initially and finally (i.e., from Eq. 10.3 $\zeta(t) = [s(t),u_0(t),u_1(t),\ldots, u_{k-1}(t)]^T$ where $s(t)$ is known initially and finally, however, $u_0(t),u_1(t),\ldots, u_{k-1}(t)$ are free to be specified initially and finally), leading to a linear two-point boundary-value problem. The solution for Eq. 10.6 follows on defining the merged state vector

$$x(t) = [\zeta(t),\lambda(t)]^T \tag{10.7}$$

leading to first-order differential equation

$$\dot{x}(t) = \Omega x(t) \tag{10.8}$$

where the constant coefficient matrix is

$$\Omega = \begin{bmatrix} \bar{A} & -\bar{B}R^{-1}\bar{B}^T \\ -Q & -\bar{A}^T \end{bmatrix}$$

The solution for $x(t)$ follows as

$$x(t) = e^{\Omega(t-t_o)}x(t_o) \tag{10.9}$$

where $e^{(\cdot)}$ is the $(4N + 2kN_c)$ by $(4N + 2kN_c)$ exponentional matrix. Comparing Eqs. 9.33 and 10.9 it is clear that the computational penalty associated with considering a control derivative penalty approach for the control problem is the increased dimension of the state/co-state system.

Equation 10.9 can be evaluated at the final time and cast in the partitioned form

$$\begin{Bmatrix} \zeta(t_f) \\ \lambda(t_f) \end{Bmatrix} = \begin{bmatrix} \phi_{\zeta\zeta} & \phi_{\zeta\lambda} \\ \phi_{\lambda\zeta} & \phi_{\lambda\lambda} \end{bmatrix} \begin{Bmatrix} \zeta(t_o) \\ \lambda(t_o) \end{Bmatrix} \tag{10.10}$$

where $\lambda(t_o)$ and $\lambda(t_f)$ are the unknown vectors and $\phi(t_f,t_o) = e^{\Omega(t_f-t_o)}$. By carrying out the partitioned matrix multiplication in for $\zeta(t_f)$, the solution for $\lambda(t_o)$ can be shown to be

$$\phi_{\zeta\lambda}\lambda(t_o) = \zeta(t_f) - \phi_{\zeta\zeta}\zeta(t_o) \qquad (10.11)$$

which is a linear equation in $\lambda(t_o)$. Equation 10.11 is inverted to yield $\lambda(t_o)$ by using Gaussian elimination or some other linear equation method. The time histories for the augmented state and co-state are recursively generated at discrete time steps by the following difference equation:

$$x_{r+1} = e^{\Omega\Delta t}x_r \quad , \quad r = 0,1,\ldots,N_s-1$$

where $x_r(t)$ denotes the merged state at time $t_r = r\Delta t + t_o$, $\Delta t = (t_f - t_o)/N_s$, and N_s is an integer which specifies the number of discrete times at which the solution for $x(t)$ is required.

Defining the vector of control and control-rates as

$$\bar{u}(t) = [u_o(t), u_1(t), \ldots, u_{k-1}(t)]^T$$

it follows that the terminal boundary conditions for $\bar{u}(t_o)$ and $\bar{u}(t_f)$ in Eq. 10.11 have yet to be specified; however, the following two choices for $\bar{u}(t_o)$ and $\bar{u}(t_f)$ naturally suggest themselves. First, for many maneuvers (for which the vehicle is not accelerating at the final time) it is convenient to have the control input nominally zero initially and finally. This is accomplished by setting $\bar{u}(t_o) = \bar{u}(t_f) = 0$ in Eq. 10.11. This choice for $\bar{u}(t_o)$ and $\bar{u}(t_f)$ has the attractive feature of eliminating the terminal jump discontinuities in the control and control-rates appearing in $\bar{u}(t)$ through k-1 time derivatives; however, terminal jump discontinuities appear for all orders of the control time derivatives greater than or equal to k. As a result, the integrating action of the derivative penalty method rapidly rolls off the high frequency content of the control.

Second, if the spacecraft is to engage and track a moving target at the end of the maneuver, then in general $\bar{u}(t_f) \neq 0$ (see Figure 10.3). For example, in the case of an in-plane target engagement as considered here, it is reasonable that the terminal control and control rates be specified consistent

with the kinematics of the estimated target motion, as follows:

$$u(t_f) = f(\hat{\theta}_{target}(t_f), \dot{\hat{\theta}}_{target}(t_f), \ldots, \hat{\theta}^{(m)}_{target}(t_f), t_f)$$

where m denotes the highest estimated time derivative used to specify the final target motion. To obtain a functional form for the terminal control, we impose the constraint that the spacecraft's attitude motion osculate the target attitude motion through (k+1)* time derivatives. In addition, since it is desirable to have the vehicle elastically at rest at the end of the maneuver, the modal amplitudes and amplitude rates are assumed to be zero through (k+1) time derivatives. It should be observed, however, that the kinematic constraints in Table 10.2 can be imposed exactly, while on the other hand, the final dynamic constraints can only be imposed approximately (e.g., by solving the equations of motion in a least-square sense for the terminal controls which

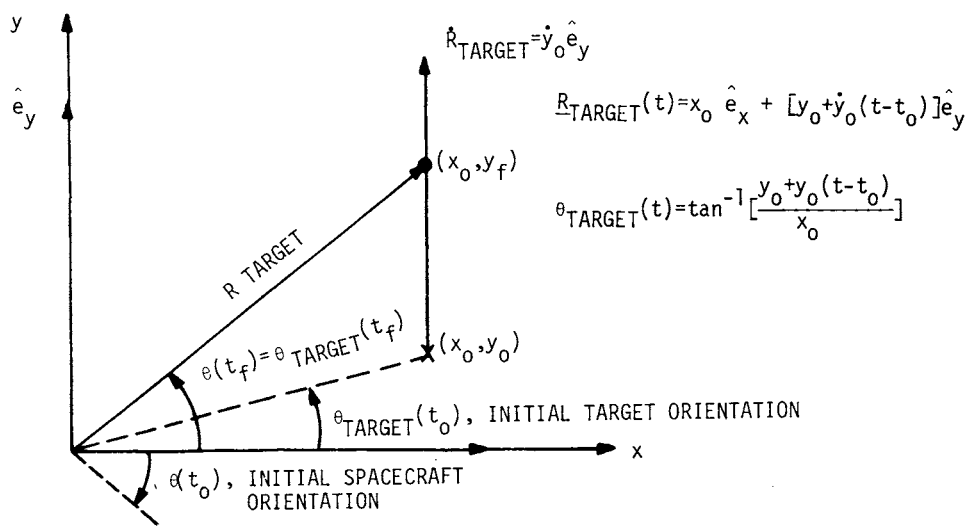

Figure 10.3 Geometry for the Target Acquisition/Tracking Maneuver

*k corresponds to the highest time derivative of the control penalized in the performance index of Eq. 10.5.

best match these boundary conditions; a least-square solution is generally required since the control influence matrix is rectangular).

To find a least-squares approximation for $\bar{u}(t_f)$, we consider the equation of motion given by:

$$M\ddot{\xi}(t) + K\xi(t) = Pu(t) \tag{10.12}$$

where M, K, and P are defined by Eq. 10.1. Introducing the kinematic and dynamic constraints of Table 10.2 into Eq. 10.12, we find

$$M\ddot{v}(t_f) + Kv(t_f) = Pu_o(t_f) \tag{10.13}$$

where

$$v(t_f) = [\hat{\theta}_{target}(t_f), 0]^T \quad , \quad u_o(t_f) = u(t_f)$$

TABLE 10.2

TERMINAL CONSTRAINTS FOR ENGAGING AND TRACKING A MOVING TARGET

Osculation and Vibration Suppression Constraints	
Kinematic Constraints*	Dynamic Constraints**
$\theta(t_f) = \hat{\theta}_{target}(t_f)$	$\ddot{\theta}(t_f) = \ddot{\hat{\theta}}_{target}(t_f)$
$\dot{\theta}(t_f) = \dot{\hat{\theta}}_{target}(t_f)$	$\theta^{(3)}(t_f) = \hat{\theta}^{(3)}_{target}(t_f)$
$\eta(t_f) = \dot{\eta}(t_f) = 0$	$\vdots$
	$\theta^{(k+1)}(t_f) = \hat{\theta}^{(k+1)}_{target}(t_f)$
	$\ddot{\eta}(t_f) = \eta^{(3)}(t_f) = \ldots = \eta^{(k+1)}(t_f) = 0$

*"^" denotes a measured or estimated quantity.

**$(\cdot)^{(n)} = \dfrac{d^n}{dt^n}(\cdot)$

The weighted least-squares solution for $u(t_f)$ in Eq. 10.13 follows as:

$$u_o(t_f) = \tilde{\tilde{P}}\hat{\theta}_{target}(t_f)$$

where

$$\tilde{P} = (P^T W P)^{-1} P^T W \begin{bmatrix} \hat{I} \\ M_{\theta n} \end{bmatrix}, \quad P = \begin{bmatrix} I & 4r^T \\ 0 & F \end{bmatrix}$$

$$W = \text{Diag.}\ (W_{11}, W_{22}, \ldots, W_{NN})$$

and W denotes the least-squares weighting matrix which is assumed to be diagonal. To impose the higher-order kinematic constraints in Table 10.2 we simply take the time derivative of Eq. 10.13, yielding

$$u_r(t_f) = \tilde{\tilde{P}}\hat{\theta}^{(r+2)}_{target}(t_f) \quad , \quad r = 0,1, \ldots, k-1 \quad (k \geq 1) \tag{10.14}$$

where $u_r(t)$ is defined by Eq. 10.3 and the least-squares weighting matrix, W, in the least squares operator of Eq. 10.14 now penalizes the higher-order rigid body and modal amplitude time derivatives.

Subject to Eqs. 10.13 and 10.14, the control boundary conditions for $\bar{u}(t)$ follow as:

$$\bar{u}(t_o) = 0 \tag{10.15}$$

$$\bar{u}(t_f) = [u_o(t_f), \ldots, u_{k-1}(t_f)]^T \tag{10.16}$$

Substituting Eqs. 10.15 and 10.16 into Eq. 10.11, and solving for $\lambda(t_o)$ yields the initial conditions necessary for optimally slewing to engage and track a moving target.

10.4.4 Target Tracking Maneuvers With Free Final Time

The natural generalization of the results of the previous section consists of allowing the final maneuver stop time to be determined as a part of the optimal solution, where $\varsigma(t_f)$ lies on the moving point $\psi(t_f)$ and the structural deformations are assumed to be zero. Subject to the performance index of Eq.

10.4, the transversality condition governing this class of spacecraft maneuvers can be shown to be (see Chapter 6)

$$-\lambda^T(t_f)\delta\zeta(t_f) + H(t_f)\delta t_f = 0$$

where $H(t_f)$ is Hamiltonian functional of Eq. 10.5. Since $\zeta(t_f)$ is supposed to lie on a moving point located by the vector function $\psi(t)$, it follows that $\delta\zeta(t_f)$ and δt_f are related as follows

$$\delta\zeta(t_f) \triangleq \frac{d\psi(t_f)}{dt}\,\delta t_f$$

Introducing the expression above into the transversality condition, yields:

$$[-\lambda^T(t_f)\,\frac{d\psi(t_f)}{dt} + H(t_f)]\delta t_f = 0$$

Since δt_f is arbitrary, the desired free-final time transversality condition is given by

$$G(t_f) = -\lambda^T(t_f)\,\frac{d\psi(t_f)}{dt} + H(t_f) = 0 \qquad (10.17)$$

where $\psi(t_f)$ can be shown to be

$$\psi(t_f) = [E^T M\mu(t_f) \quad , \quad E^T M\dot{\mu}(t_f) \quad , \quad \bar{u}(t_f)]^T$$

$$\mu(t_f) = \hat{\theta}_{target}(t_f)[1,0]^T \quad (Nx1)$$

and $\bar{u}(t_f)$ is defined by Eqs. 10.14 and 10.16, and $\mu(t_f)$ is a vector which specifies the target motion.

Several observations about Eq. 10.17 immediately follow: (i) $G(t_f)$ is nonlinear; (ii) $G(t_f)$ is a function of the target motion, the state, state and control time derivatives, and (iii) there is no immediately obvious starting guess for the desired final time. To find a starting iterative for t_f, however, we can exploit the fact that the performance index of Eq. 10.4, taken as a function of t_f, has a minimum value for the time, t_f^*, which satisfies Eq. 10.17. In order to efficiently sweep through many candidate values of t_f, we first obtain a closed-form solution for the performance index, $J(t_f)$. The

first step consists of writting Eq. 10.4 as

$$J(t_f) = \frac{1}{2}\int_0^{t_f} [\zeta^T Q \zeta + \lambda^T \bar{B} R^{-1} \bar{B}^T \lambda] dt \tag{10.18}$$

where the control, $u_k(t)$, has been replaced by the co-state, $\lambda(t)$, by using the equation $u_k(t) = -R^{-1}\bar{B}^T\lambda(t)$. Equation 10.18 is further simplified by recalling the definition for the merged state vector, $x(t)$, of Eqs. 10.7 and 10.9, leading to

$$J(t_f) = \frac{1}{2} x_o^T \left(\int_0^{t_f} e^{\Omega^T t} W e^{\Omega t} dt\right) x_o \tag{10.19}$$

where W = Block Diag. $[Q, \bar{B}R^{-1}\bar{B}^T]$.

As shown by Van Loan (ref. 18), the integral of exponential matrices in Eq. 10.19 can be computed by defining the constant matrix

$$\Upsilon = \begin{bmatrix} -\Omega^T & W \\ 0 & \Omega \end{bmatrix}$$

and evaluating the matrix exponential

$$e^{\Upsilon t_f} = \begin{bmatrix} F_1(t_f) & G_1(t_f) \\ 0 & F_2(t_f) \end{bmatrix} \tag{10.20}$$

where Van Loan establishes that

$$F_1(t_f) = e^{-\Omega^T t_f}, \quad F_2(t_f) = e^{\Omega t_f}, \quad G_1(t_f) = e^{-\Omega^T t_f} \int_0^{t_f} e^{\Omega^T t} W e^{\Omega t} dt$$

from which it follows that the integral of Eq. 10.19 can be calculated from the matrix exponential of Eq. 10.20 as

$$J(t_f) = \frac{1}{2} x_o^T F_2^T(t_f) G_1(t_f) x_o \tag{10.21}$$

In order to efficiently evalute Eq. 10.21 for many values of the final time, we exploit the semi-group properties of exponential matrices and write the following recursive difference equations for the matrix partitions of Eq. 10.20:

$$F_1(t_f + \Delta t) = F_1(t_f)F_1(\Delta t) \tag{10.22a}$$

$$F_2(t_f + \Delta t) = F_2(t_f)F_2(\Delta t) \tag{10.22b}$$

$$G_1(t_f + \Delta t) = F_1(t_f)G_1(\Delta t) + G_1(t_f)F_2(\Delta t) \tag{10.22c}$$

where Δt is the desired incremental change in the final maneuver time. In addition, the initial condition for the merged state vector, x_o, in Eq. 10.21 is an implicit function of the target motion and must be computed for each new value of the final time $t_f + \Delta t$. To see this we observe that $\lambda(t_o)$ is obtained from Eq. 10.11 as

$$\phi_{\zeta\lambda}\lambda(t_o) = \zeta^*(t_f) - \phi_{\zeta\zeta}\zeta(t_o) \tag{10.23}$$

where

$$\zeta^*(t_f) = [E^T M\nu(t_f) \quad , \quad E^T M\dot{\nu}(t_f) \quad , \quad \bar{u}(t_f)]$$

$\nu(t_f)$ is defined by Eq. 10.13 and $\bar{u}(t_f)$ is defined by Eqs. 10.14 and 10.16. As a result the initial merged state vector, x_o, can be written as

$$x_o = [\zeta(t_o) \quad , \quad [\phi_{\zeta\lambda}]^{-1}\{\zeta^*(t_f) - \phi_{\zeta\zeta}\zeta(t_o)\}]^T$$

where x_o is an explicit function of the final time.

Subject to the recursion relationships of Eq. 10.22, the matrix partitions for $\phi_{\zeta\lambda}$ and $\phi_{\zeta\zeta}$ are obtained from Eq. 10.22b, since $F_2(t_f) \triangleq \phi(t_f,t_o)$ as defined by Eq. 10.10. Moreover, we observe that for each new choice for t_f, new estimates are required for $\hat{\theta}_{target}(t_f)$, $\dot{\hat{\theta}}_{target}(t_f),\ldots,\hat{\theta}^{k+1}_{target}(t_f)$. This kinematic information is used to compute $\psi(t_f)$ in Eq. 10.17, and $\zeta^*(t_f)$ in Eq. 10.23.

In order to recursively evaluate the transversality condition of Eq. 10.17, we write the Hamiltonian functional of Eq. 10.5 as

$$H(t_f) = \frac{1}{2} x_o^T e^{\Omega^T t_f} W' e^{\Omega t_f} x_o$$

or

$$H(t_f) = \frac{1}{2} x_o^T F_2^T(t_f) W' F_2(t_f) x_o \tag{10.24}$$

where

$$W' = \begin{bmatrix} Q & A \\ \bar{A} & -\bar{B}R^{-1}\bar{B}^T \end{bmatrix}$$

The numerical values required for $\lambda(t_f)$ in Eq. 10.17 follow from Eq. 10.11 as

$$\lambda(t_f) = \phi_{\lambda\zeta}\zeta(t_o) + \phi_{\lambda\lambda}\lambda(t_o) \tag{10.25}$$

where the matrix partitions $\phi_{\lambda\zeta}$ and $\phi_{\lambda\lambda}$ are obtained from 10.22b and the solution for $\lambda(t_o)$ is obtained from Eq. 10.23.

The basic algorithm consists of: (i) selecting an initial maneuver time; (ii) selecting a time increment Δt for propagating $F_1(t_f)$, $F_2(t_f)$, $G_1(t_f)$, $\Psi(t_f)$, $\lambda(t_o)$, $\lambda(t_f)$, $J(t_f)$, $H(t_f)$, $\zeta^*(t_f)$ and the transversality condition $G(t_f)$; (iii) solving for x_o at time $t^{k+1} = t^k + \Delta t$; (iv) carrying out a coarse grid search for a finite final time which minimizes $J(t_f)$; and (v) iteratively solving for the optimal final time by minimizing $G(t_f)$ in Eq. 10.17. In order to establish a successive approximation strategy for iteratively refining an approximate value of $\hat{t}_f$, we write $G(t_f)$ as

$$G(\hat{t}_f + \Delta t) = 0 \tag{10.26}$$

where $\hat{t}_f + \Delta t$ is the correct optimal final time.

Expanding Eq. 10.26 to first-order, we obtain

$$0 \approx G(t^k) + \frac{\partial G}{\partial t_f^k} \Delta t$$

which can be solved for the (k+1)th approximation for t_f^{k+1}, yielding the Newton algorithm

$$t_f^{k+1} = t_f^k - G(t_f^k)/\left(\frac{\partial G}{\partial t_f^k}\right) \tag{10.27}$$

where $t_f^o = \hat{t}_f$, $\frac{\partial G}{\partial t_f^k}$ is obtained from the finite difference approximation

$$\frac{\partial G}{\partial t_f^k} = [G(t_f^k + \varepsilon) - G(t_f^k)]/\varepsilon$$

and $\varepsilon \cong t_f^{k-1} \times 10^{-4}$ is a typical perturbation in the final time. Equation (10.27) is iterated until $|t_f^{k+1} - t_f^k| \leq \sigma$ where σ is a small convergence tolerance. An example maneuver is provided in Section 10.5.

10.4.5 Free Final Angle Maneuvers Using the Control-Rate Penalty Method

Since the free final angle transversality condition is naturally defined in terms of physical (configuration) rather than modal coordinates (the results of this section are analogous to those of Section 9.4.4), the following two transformation equations permit the use of the formulation presented in Section 10.4.3. First, the modal space state transition matrix, $\phi(t_f,t_o)$, of Eq. 10.9 is mapped to configuration space via the transformation (refs. 4,16):

$$\Phi(t_f,t_o) = \Theta\phi(t_f,t_o)\Theta^{-1} \tag{10.28}$$

where

Θ = Block Diag. [E,E,I,ME,ME,I]

Θ^{-1} = Block Diag. [E^TM,E^TM,I,E^T,E^T,I]

I is an $kN_C \times kN_C$ identity matrix, M is defined by Eq. 10.1, and E is defined by Eq. 10.2.

Second, once the configuration space initial conditions have been obtained, the modal space initial conditions are obtained from the transformation

$$\begin{Bmatrix} s(t_o) \\ \lambda(t_o) \end{Bmatrix} = \Theta^{-1} \begin{Bmatrix} \Sigma(t_o) \\ \Lambda(t_o) \end{Bmatrix} \tag{10.29}$$

where $\Sigma(t)$ as the augmented configuration space state and $\Lambda(t)$ as the augmented physical space co-state. The solution for the configuration space free final angle problem is obtained by using the transversality conditions presented in Section 6.2.

The configuration space boundary conditions for the free final angle problem are given by

$$\Sigma(t_o) = [\theta(t_o),\ \eta(t_o),\ \dot{\theta}(t_o),\ \dot{\eta}(t_o),\ \bar{u}(t_o)]^T \tag{10.30a}$$

$$\Sigma(t_f) = [\theta(t_f),\ \eta(t_f),\ \dot{\theta}(t_f),\ \dot{\eta}(t_f),\ \bar{u}(t_f)]^T \tag{10.30b}$$

where

$$\theta(t_f) = \text{free}$$

and the following constraints have been imposed in the example maneuvers of Section 10.5:

$$\eta(t_o) = \eta(t_f) = 0 \tag{10.31a}$$

$$\dot{\eta}(t_o) = \dot{\eta}(t_f) = 0 \tag{10.31b}$$

$$\bar{u}(t_o) = \bar{u}(t_f) = 0 \tag{10.31c}$$

Since the final angle is assumed to be free, the transversality condition providing the replacement boundary condition for the final angle follows as:

$$-\Lambda^T(t_f)\ \delta\Sigma(t_f) = 0 \tag{10.32}$$

where $\delta\Sigma(t_f)$ is the variation of the configuration space state. Since θ_f is free and $\dot{\theta}_f$, η_f, $\dot{\eta}_f$, and $\bar{u}(t_f)$ are specified, $\delta\Sigma(t_f)$ in Eq. 10.32 can be written as

$$\begin{aligned}\delta\Sigma(t_f) &= [\delta\theta(t_f),\delta\eta(t_f),\delta\dot{\theta}(t_f),\delta\dot{\eta}(t_f),\delta\bar{u}(t_f)] \\ &= [\delta\theta(t_f),0,0,0,0]\end{aligned} \tag{10.33}$$

Substituting Eq. 10.33 into Eq. 10.32, leads to

$$-\Lambda_1(t_f)\delta\theta(t_f) = 0$$

where $\Lambda_1(t_f)$ is the first element of $\Lambda(t_f)$. Since $\delta\theta(t_f)$ is arbitrary, it follows that

$$\Lambda_1(t_f) = 0$$

Accordingly, $\theta(t_o)$, $\eta(t_o)$, $\dot{\theta}(t_o)$, $\dot{\eta}(t_o)$, $\bar{u}(t_o)$, $\Lambda_1(t_f)$, $\eta(t_f)$, $\dot{\theta}(t_f)$, $\dot{\eta}(t_f)$, and $\bar{u}(t_f)$ provide the $4N + 2kN_c$ boundary conditions necessary for specifying the augmented configuration space free final angle maneuver control problem.

10.4.5 Solution for the Initial Co-States for the Free Final Angle Maneuver Problem

The solution for the free final angle optimal control problem can be cast in the form

$$\mathbf{y}(t_f) = \Phi(t_f,t_o)\ \mathbf{y}(t_o) \tag{10.33}$$

where $\Phi(t,t_o)$ is the physical space state transition matrix defined in Eq. 10.28 and $\mathbf{y}(t)$ is given by

$$\mathbf{y}(t) = [\Sigma(t),\ \Lambda(t)]^T = [y_1(t),y_2(t),\ldots,y_{4N+2kN_c}(t)]^T \tag{10.34}$$

where $\Lambda(t_o)$ is unknown in Eq. 10.33.

The linear equation defining the solution for $\Lambda(t_o)$ follows on carrying out the partitioned matrix multiplication for $y_2(t_f),\ldots,y_{N'+1}(t_f)$ in Eq. 10.33, where $N' = 2N + kN_c$; leading to:

$$D\Lambda(t_o) = \sigma_f - C\sigma_o \tag{10.35}$$

where

$$\sigma_o = [y_1(t_o)\ldots y_{N'}(t_o)]^T$$

$$\sigma_f = [y_2(t_f)\ldots y_{N'+1}(t_f)]^T$$

$$C_{i-1,j} = \Phi_{ij}(t_f,t_o)\ ,\quad (i = 2,\ldots,N'+1;\ j = 1,\ldots,N')$$

$$D_{i-1,j-N'} = \Phi_{ij}(t_f,t_o)\ ,\quad (i = 2,\ldots,N'+1;\ j = N'+1,\ldots,2N')$$

Equation 10.35 is solved for $\Lambda(t_o)$ using Gaussian elimination or other suitable algorithms for linear equations.

The time histories for the state and control are obtained most efficiently by using the recursive formulas following Eq. 10.11, subject to the initial state and co-state boundary conditions provided by Eqs. 10.29 and 10.35.

10.4.6 Weighting Matrix Specification in the Control-Rate Penalty Formulation

In the example maneuvers of Section 10.5 the following block diagonal matrices have been used for the control-rate penalty weighting matrices Q and R in Eq. 10.4.

$$Q = \text{Block Diag}\ [Q_{ss},Q_{oo},\ldots,Q_{k-1,k-1}]$$

where

$$Q_{ss} = \gamma_{ss} I_s,\ I_s = \text{Diag}(10^{-2},1,1,\ldots,1) \quad , \quad (2Nx2N)$$

$$Q_{pp} = \gamma_{pp} I_p, I_p = \text{Diag}(10^{-3},1,1,\ldots,1) \quad , \quad (N_c x N_c)$$

$$R = \gamma_{rr} I_r,\ I_r = \text{Diag}(10^{-3},1,1,\ldots,1) \quad , \quad (N_c x N_c)$$

for $p = 0,1,\ldots,k-1$ and γ_{ss}, γ_{pp}, and γ scalar weights.

Since it is desirable to not penalize the rigid body motion in the state weighting matrix Q_{ss} (since the maneuver angle size is dictated by the boundary conditions $\theta(t_o),\theta(t_f)$), we set the first element to be two orders of magnitude less than the penalties on $\dot{\theta}(t)$, $\eta(t)$ and $\dot{\eta}(t)$. The first element of Q_{ss} is not set to zero because this causes repeated zero eigenvalues in the state/co-state system matrix, Ω, of Eq. 10.8, which can potentially lead to numerical difficulties in calculating the exponential matrix.

The value of γ_{pp} in Q_{pp} determines participation of the rigid hub and appendage controllers in the optimal solution. In particular, since it is desirable to have the rigid hub controller execute most of the slewing maneuver while the appendage controls function principally as vibration suppressors, the first element of I_p is set to provide two or three orders of magnitude smaller penalty on the rigid hub control.

In addition, it has been found that by adjusting the norms of the weighting matrices Q_{ss}, Q_{oo}, and Q_{ii} for $i = 0, \ldots, k-1$ to be several orders of magnitude smaller than the norm of R, the eigenvalue bandwidth of Ω in Eq. 10.8 can be significantly reduced. As a result, the time interval over which the optimal solution can be reliably obtained is increased. However, the decrease in the eigenvalue bandwidth of Ω are usually obtained at the expense of increased peak flexural deformations during the maneuver.

10.4.7 Evaluation of the Response of a Residual Plant Model

In order to investigate the possibility of control spillover effects which can excite the response of the previously truncated plant dynamics models, we

must integrate a system of equations consisting of the state (used for the control design), co-state, and residual state differential equations. Assuming that the residual plant dynamics equation can be written as

$$\begin{aligned}\dot{s}_r &= A_r s_r + B_r u \\ &= A_r s_r + B_r S_u \zeta \quad , \quad s_r(t_o) \text{ given}\end{aligned} \tag{10.35}$$

where A_r is the residual plant dynamics matrix, B_r is the residual control influence matrix, S_u = Block $[\bar{0},I,0,\ldots,0]$ is an N_c x $(2N + kN_c)$ selection operator for the control, $\bar{0}$ is an N_c x $2N$ null matrix, I is an N_c x N_c identity matrix, and 0 is an N_c x N_c null matrix. The system response is obtained by defining the merged state vector for Eqs. 10.6 and 10.35:

$$z(t) = [\zeta(t), \lambda(t), s_r(t)]^T \tag{10.36}$$

leading to the first-order differential equation

$$\dot{z}(t) = \Xi z(t) \tag{10.37}$$

where the constant coefficient matrix is

$$\Xi = \begin{bmatrix} \bar{A} & -\bar{B}R^{-1}\bar{B}^T & 0 \\ -Q & -\bar{A}^T & 0 \\ B_r S_u & 0 & A_r \end{bmatrix}$$

The solution for z(t) follows as

$$z(t) = e^{\Xi(t-t_o)} z(t_o) \tag{10.38}$$

where $z(t_o) = [\zeta(t_o), \lambda(t_o), s_r(t_o)]^T$ and $\lambda(t_o)$ is provided by Eq. 10.11. The time histories for the augmented state, co-state, and residual state are recursively generated at discrete time steps by the following difference equation:

$$z_{r+1} = e^{\Xi \Delta t} z_r \quad , \quad r = 0,1,\ldots,N-1$$

where z_r denotes the merged state at time $t_r = r\Delta t + t_o$, and N is an integer which specifies the numbers of discrete times at which the solution for z(t) is required.

It should further be observed that Eq. 10.35 can be obtained by truncating the system equations of motion given by Eq. 10.2, where s(t) is partitioned as

$x = [s_c, s_r]^T$

s_c denotes the controlled plant model

s_r denotes the residual (i.e. uncontrolled) plant model

10.5 EXAMPLE MANEUVERS

We now consider example maneuvers for the configuration shown in Figure 10.1, using the formulation above. For all cases we have assumed the following configuration parameters: the moment of inertia of the undeformed structure about the spin axis, $\hat{I}$, is 7000 kg-m^2; the mass/length of the four identical elastic appendages, ρ, is .4 g/m; the length of each cantilevered appendage, L, is 150 m; the flexural rigidity of each cantilevered appendage, EI, is 1500 Kg-m^3/s^2; and the radius of the rigid hub, r, is 1 m. In the integrations over the mass and stiffness distributions, the radius of the hub is not neglected in comparison to the appendage length. We have adopted as "assumed modes" the comparison functions

$$\phi_o(x - r) = 1 - \cos \frac{p\pi(x-r)}{L} + \frac{1}{2}(-1)^{p+1} \frac{p\pi(x-r)^2}{L}$$

$$(p = 1,2, \ldots, n)$$

With reference to Table 10.3 and Figures 10.4 through 10.22, we consider qualitatively the graphical summaries of the state, control, and control-rate time histories.

Case 1 (Figure 10.4) presents the optimal control solution for a rest-to-rest maneuver when control time derivatives are not penalized in the performance index. In particular, we note that the terminal controls are characterized by on/off jump discontinuities. The frequency spectra for the controls are shown in Figure 10.5. The equation for the Fourier transform is given by

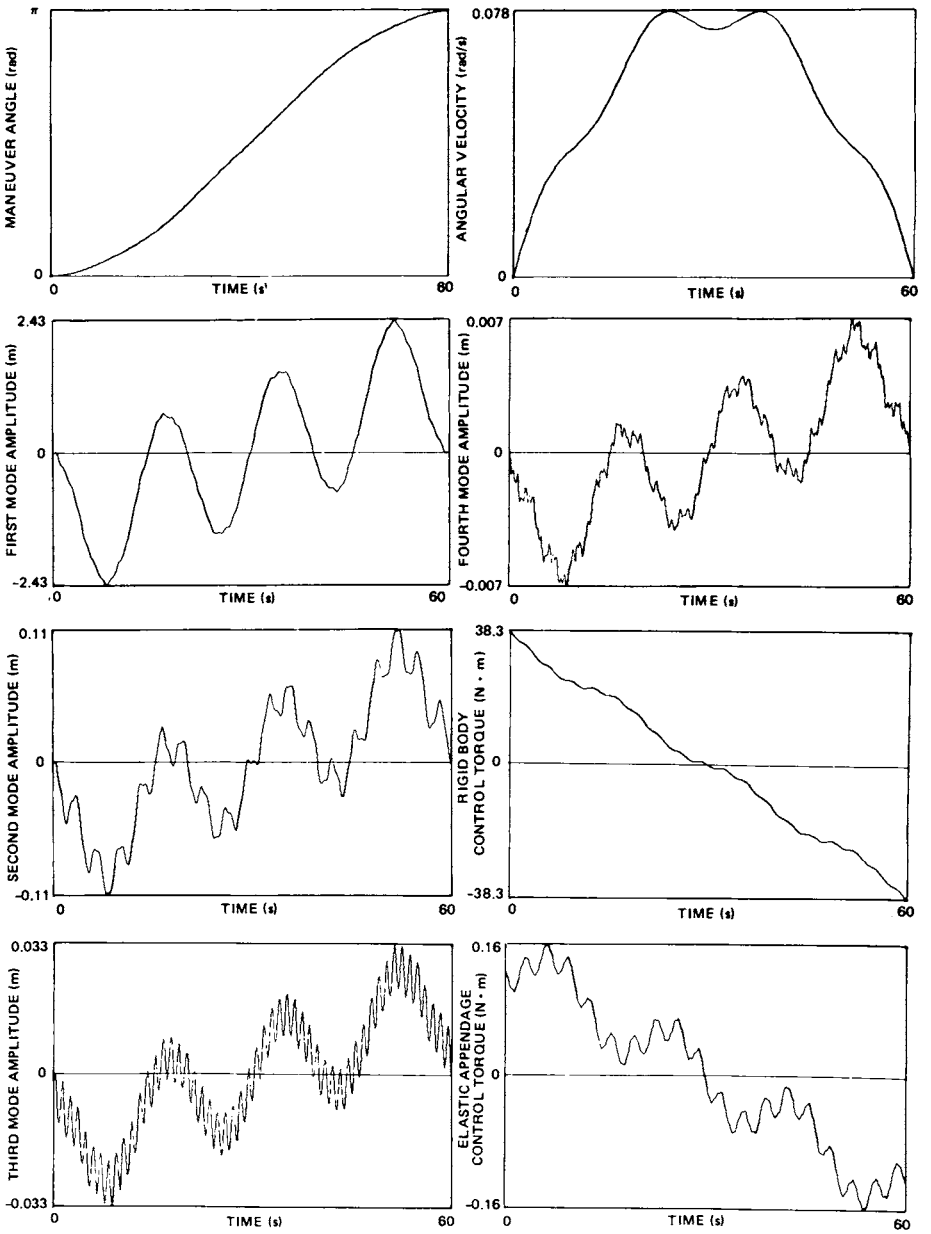

Figure 10.4 Case 1 Rest-to-Rest Maneuver, k=0, 4 Modes, 5 Controls

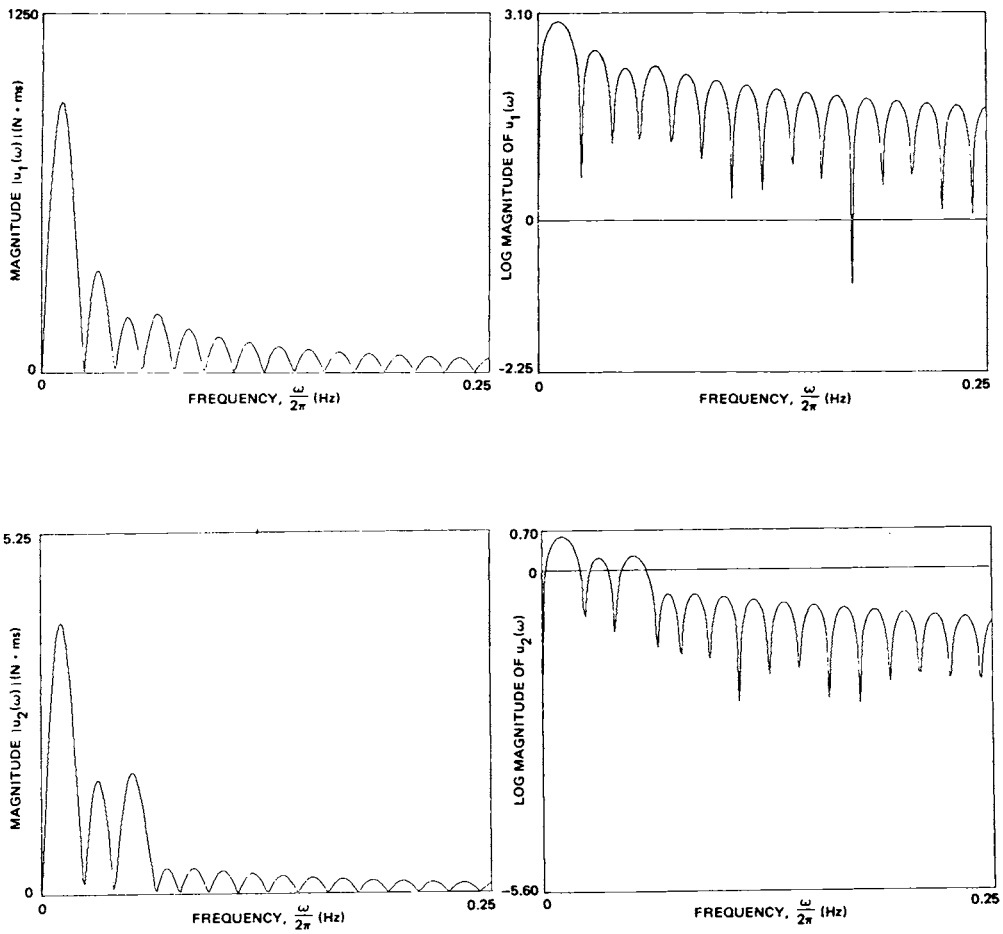

Figure 10.5 Frequency Spectra of Control Torques for Case 1

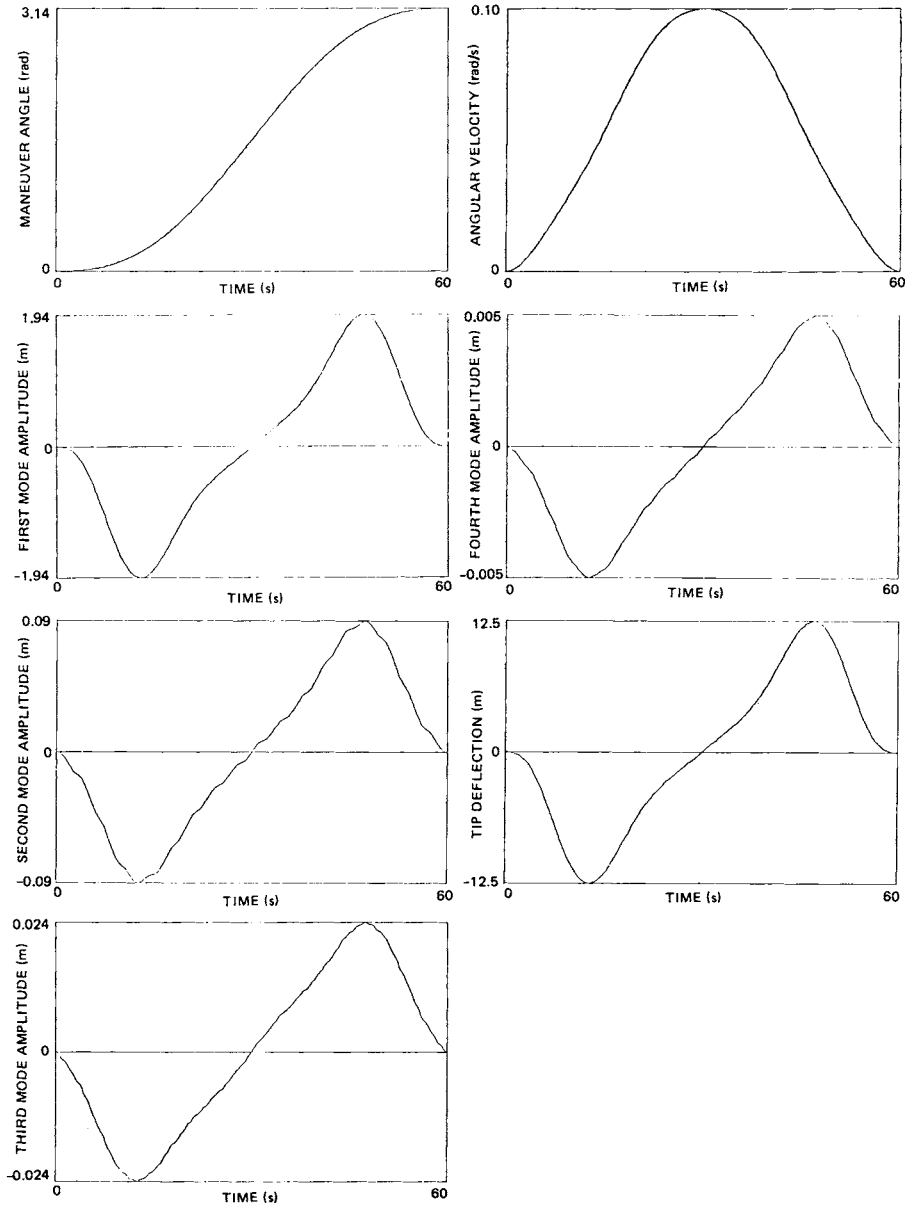

Figure 10.6 Case 2, Rest-to-Rest Maneuver k=1, 4 Modes, 4 Controls

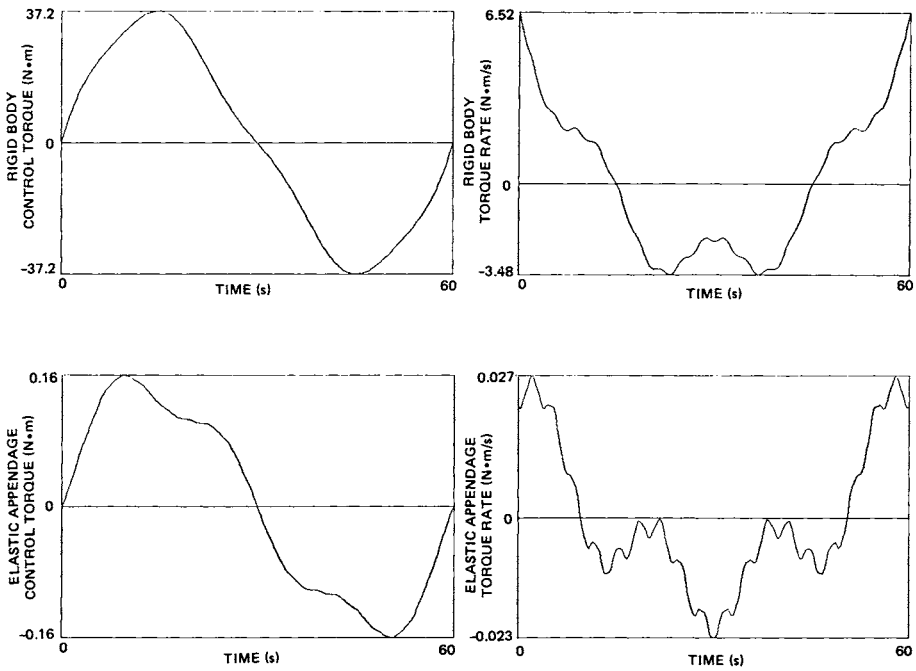

Figure 10.7 Control Torque Profiles for Case 2

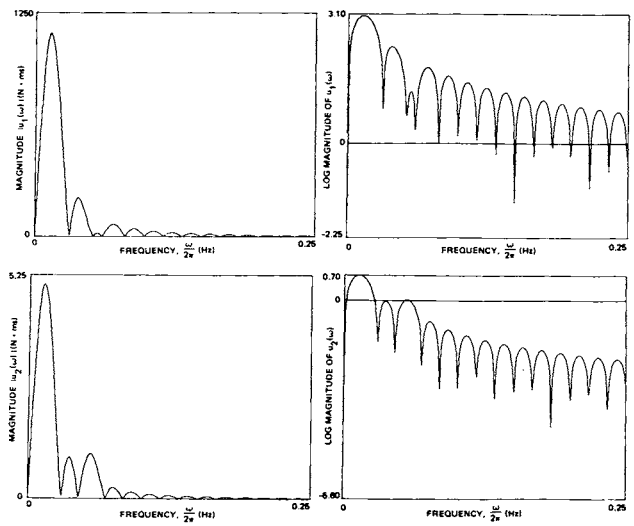

Figure 10.8 Frequency Spectra of Control Torques for Case 2

Table 10.3 Description of Test Case Maneuvers

Case No.	Maneuver Description	t_f sec	No. of modes	θ_o rad	$\dot{\theta}_o$ rad/s	θ_f rad	$\dot{\theta}_f$ rad/s	No. of Controls	k	Q_{ss}^*	Q_{00}	Q_{11}	Q_{22}	Q_{33}**
1	Rest-to-rest	60	2	0	0	π	0	5	0	$10^{-3}I^{*+}$	I^{k++}	-	-	-
2	Rest-to-rest	60	2	0	0	π	0	5	1	$10^{-3}I^*$	$10^{-9}I$	W_1	-	-
3	Rest-to-rest	60	2	0	0	π	0	5	2	$10^{-3}I^*$	$10^{-9}I$	$10^{-9}I$	W_2	-
4	Rest-to-rest	60	2	0	0	π	0	5	3	$10^{-3}I^*$	$10^{-9}I$	$10^{-9}I$	$10^{-9}I$	W_3
5	Rest-to-rest	60	4	0	0	π	0	13	0	$10^{-3}I^*$	I^k	-	-	-
6	Spin reversal	60	2	0	-0.5	2π	0.6	5	2	$10^{-3}I^*$	$10^{-9}I$	$10^{-9}I$	I^k	-
7	Free final angle spin reversal	60	2	0	-0.5	free	0.6	5	2	$10^{-3}I^*$	$10^{-9}I$	$10^{-9}I$	I^k	-
8	Slewing to engage a moving target	40	2	0	0	$\theta_T(t_f)$	$\dot{\theta}_T(t_f)$	5	2	$10^{-3}I^*$	$10^{-9}I$	$10^{-9}I$	I^k	-

+ I^* diag $(10^{-2},1,\ldots,1)(2N\times 2N)$

++ I^k diag $(10^{-2},1,\ldots,1)(N_c \times N_c)$

* The matrices shown are applied to physical space coordinates. These are mapped into modal space to form W_{ss}.

** $Q_{pp} = R$ when $\rho = k$

W_1 = diag [0.001, 2.2]

W_2 = diag [0.001, 45]

W_3 = diag [0.001, 900]

$$u_j(\omega) = \int_{-\infty}^{\infty} [\delta(t-t_o) - \delta(t-t_f)]e^{-i\omega t}u_j(t)dt,$$

$$j = 1,2 \text{ and } \delta(\sigma) = \begin{cases} 0 & \sigma < 0 \\ 1 & \sigma \geq 0 \end{cases}$$

where $u_1(t)$ is the rigid body control and $u_2(t)$ is the appendage control. A recursive numerical algorithm for computing $u_j(\omega)$ is presented in Appendix E.

Cases 2 through 5 are subject to the same maneuver time and boundary conditions used in Case 1. Cases 2 through 4 compare the resulting maneuvers as higher control time derivatives are included in the performance index. The control weight matrices for these cases are selected so that the peak appendage control torques are roughly the same as for Case 1.

Case 2 (Figures 10.6 and 10.7) have the control and the first time derivative of the control penalized in the performance index. As a result the specified control boundary conditions are given by:

$$u(t_o) = u(t_f) = 0.$$

As seen in Figure 10.6, the terminal control torque vanishes as required; thus, eliminating the usually undesirable jump discontinuity. Moreover, we can see that the modal amplitude time histories have been significantly smoothed, when compared to the corresponding results of Case 1. The improved system response has been obtained even while modestly decreasing the peak torque requirements by 3%. The reductions in the peak flexural deformations, when compared to Case 1, can be seen to be: (i) 25% less for mode one; (ii) 22% less for mode two; (iii) 38% less for mode three; and (iv) 40% less for mode four. The frequency spectra plots (Figure 10.8) for the control torques show an increase in peak magnitudes at the low end of the spectrum, with a faster roll-off for higher frequencies. This rapid roll-off in the frequency spectra of the control torques greatly reduces the problems associated with control spillover effects to the truncated elastic modes of freedom. However, the extent of control spillover minimization is highly problem dependent.

Case 3 (Figures 10.9 and 10.10) has the control and the first two derivatives of the control penalized in the performance index. As a result the specified control boundary conditions are given by:

$$u(t_0) = u(t_f) = \dot{u}(t_0) = \dot{u}(t_f) = 0.$$

As in Case 2, the terminal jump discontinuities in the control have been eliminated. Moreover, we observe that the modal amplitude time histories have been further smoothed over results of Case 2. The peak torque requirement for Case 3 is greater than for Case 2. However, the change in the peak torque from Case 2 to Case 3 is less than the change in the peak torque from Case 1 to Case 2. The reduction in the peak flexural deformations, when compared to Case 1, can be seen to be: (i) 8% for mode one; (ii) 10% for mode two; (iii) 22% for mode three; and (iv) 17% for mode four. Figure 11 shows the frequency spectra of the control torques. Compared with Case 2, the peak magnitude for the rigid body control spectrum is increased, whereas the peak magnitude for the elastic appenage control spectrum is decreased. However, both spectra show a more rapid roll-off for higher frequency when compared with Case 2.

Case 4 (Figures 10.12 and 10.13) has the control and the first three time derivatives of the control penalized in the performance index. As a result, the specified control boundary conditions are given by:

$$u(t_0) = \dot{u}(t_0) = \ddot{u}(t_0) = u(t_f) = \dot{u}(t_f) = \ddot{u}(t_f) = 0.$$

As in Cases 2 and 3, the terminal jump discontinuities in the control have been eliminated. We observe that the improvement in the system response has been achieved when compared with the previous cases; however, the increased computational cost offsets the gain in system performance. Thus, we conclude that a good trade-off between system response and the computation effort required to solve the control differential equation occurs when k = 2, as in Case 3. Figure 10.14 is the frequency spectra for the control torques. Compared with the previous cases, the peak magnitude for the rigid body control

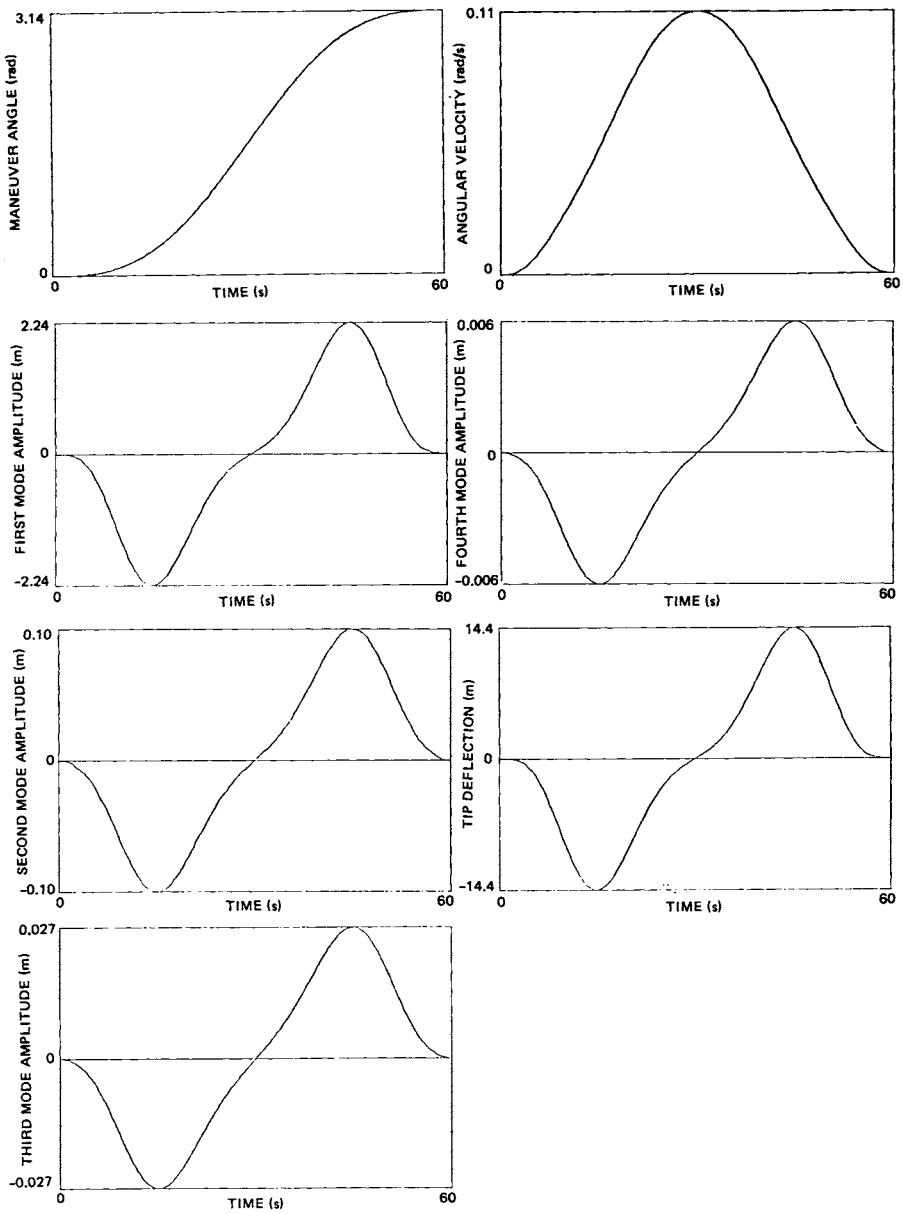

Figure 10.9 Case 3, Rest-to-Rest Maneuver, k=2, 4 Modes, 5 Controls

spectrum is further increased, and that for the elastic appendage control spectrum is further decreased. The high frequency roll-off for both spectra is the most rapid when compared with the previous cases.

Table 10.4 summarizes the changes in system response as k varies zero to four in Cases 1 through 4.

Case 5 (Figures 10.15 and 10.16) presents the optimal control formulation when control time derivatives are not penalized in the performance index, and

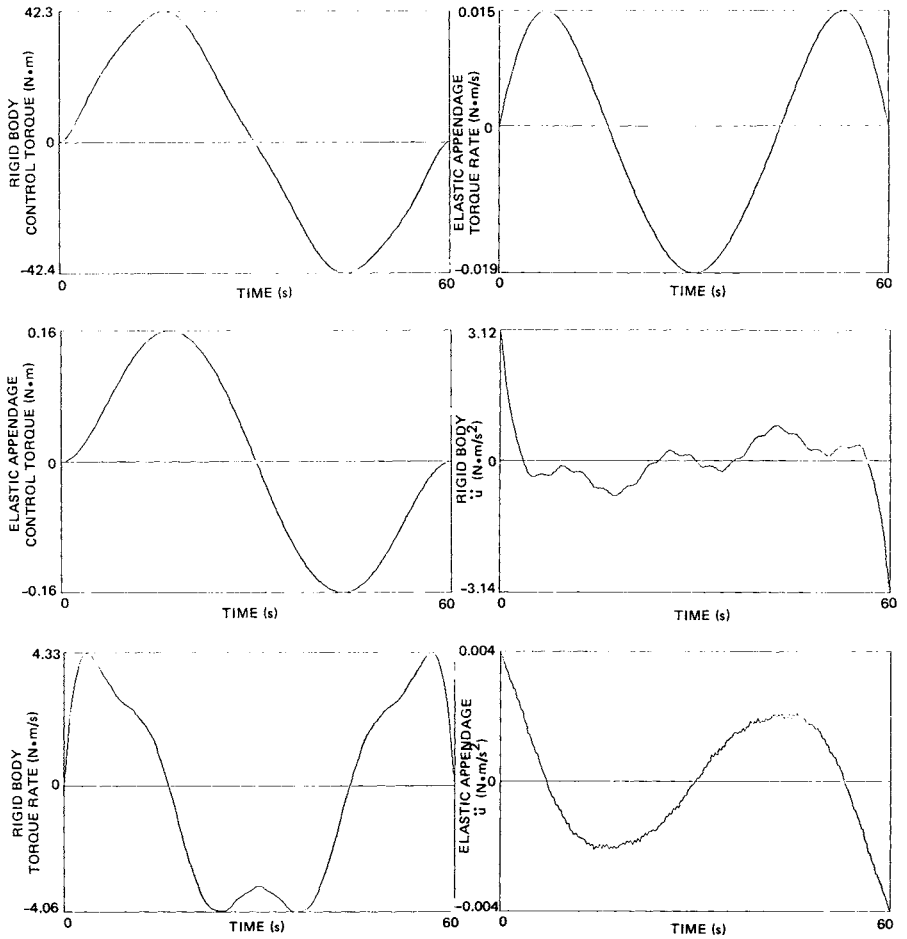

Figure 10.10 Control Torque Profiles for Case 3

multiple actuator control is employed. In particular we consider the case where each elastic appendage is assumed to have three control torque actuators, leading to a total of 13 actuators acting on the vehicle. The actuators are located at 38.5 m, 76 m, and 113.5 m from the center of the rigid hub. We observe that system response is improved over results of Case 1. However, we observe the control-rate penalty results of Cases 2 through 4 are superior to the k=0 distributed control results of Case 5 in that the time histories are

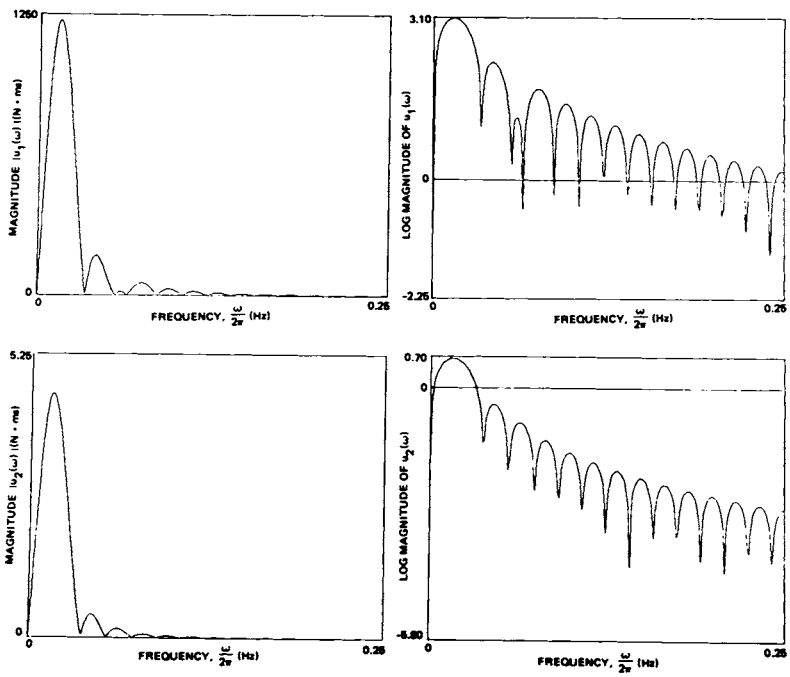

Figure 10.11 Frequency Spectra of Control Torques for Case 3

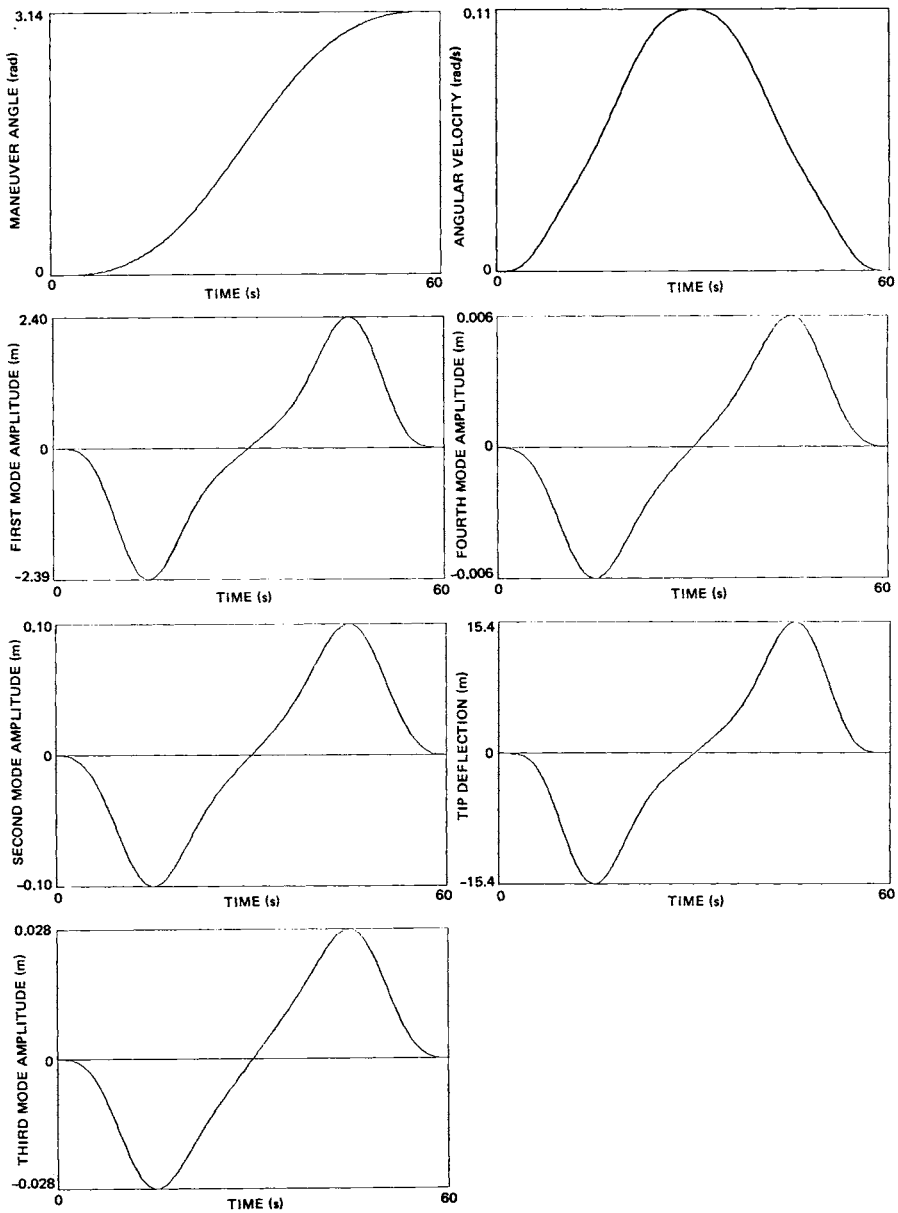

Figure 10.12 Case 4, Rest-to-Rest Maneuver, k=3, 4 Modes, 5 Controls

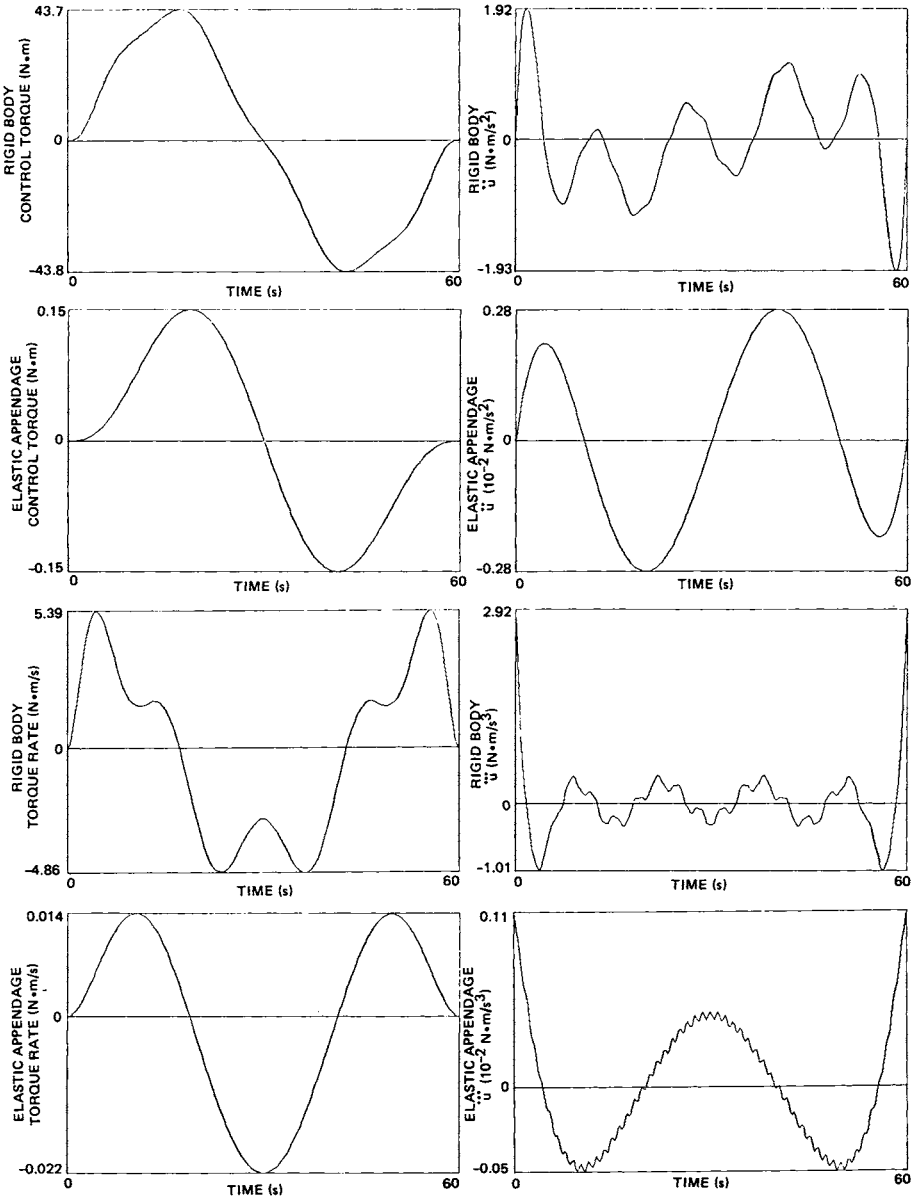

Figure 10.13 Control Torque Profiles for Case 4

much smoother. Thus, we conclude (for this application) that the use of control-rate penalties in the performance index has yielded superior system performance. However, by combining control-rate penalties and multiple control actuators, further improvements in the system response can be realized (e.g. see refs. 16 and 17).

Case 6 (Figures 10.17 and 10.18) is a spin reversal maneuver which uses distributed control and control-rate penalties through k=2. This example respresents a difficult maneuver in that the vehicle must first despin and then spinup to the desired orientation and angular rate during a fixed time interval.

The boundary conditions for Case 7 (Figures 10.19 and 10.20) are identical to Case 6, except that the final angle is free to be determined as part of the

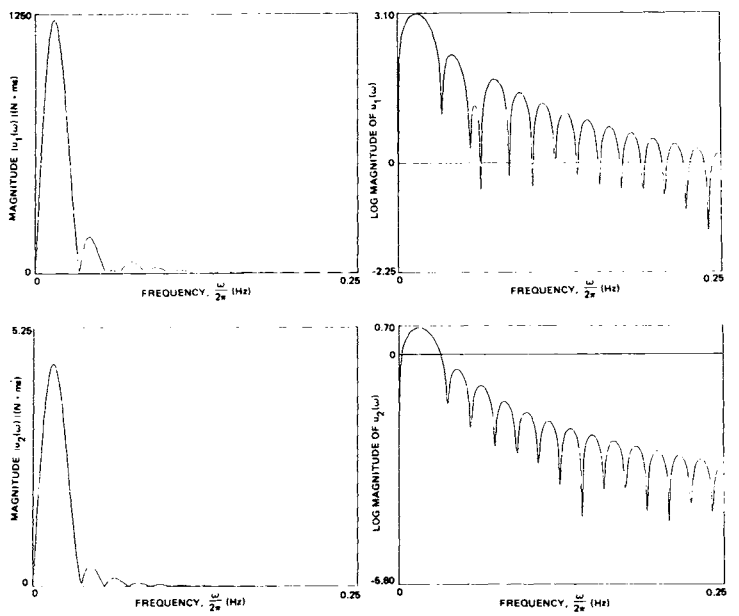

Figure 10.14 Frequency Spectra of Control Torques for Case 4

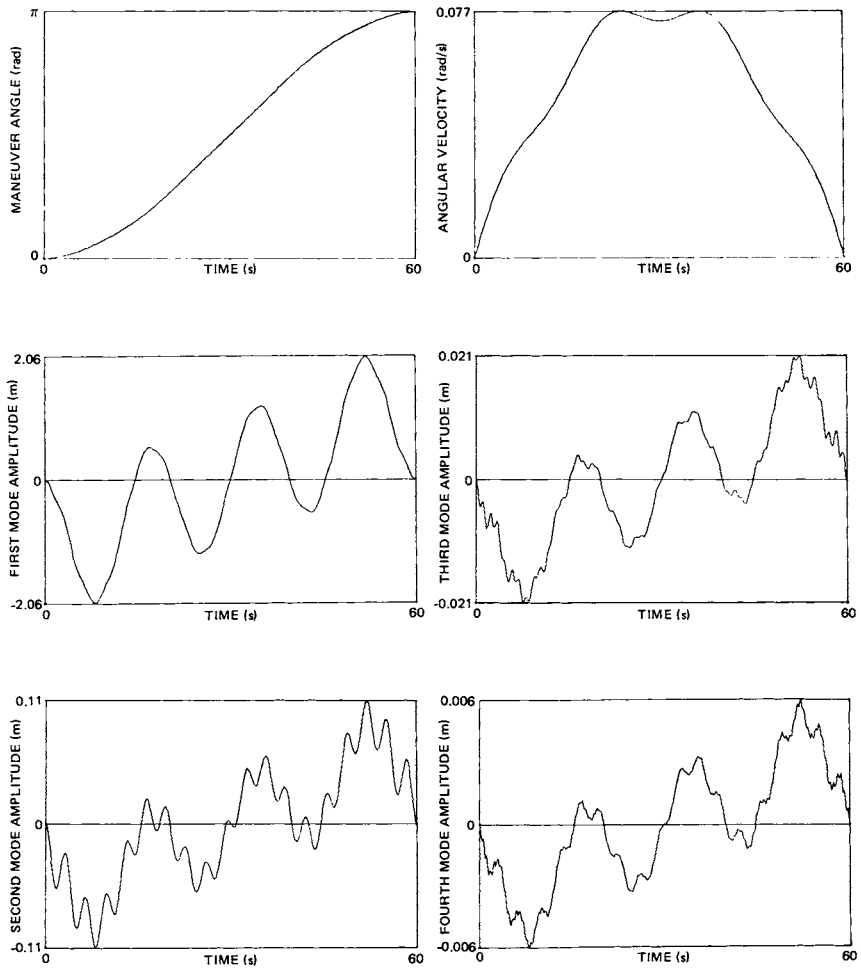

Figure 10.15 Case 5, Rest-to-Rest Maneuver, k=0, 2 Modes, 13 Controls

solution. We observe on comparing the results of Cases 6 and 7, that both the peak torque requirement and peak structural deformations are significantly reduced for the results of Case 7. The results of Case 7 are superior to the results of Case 6 because the free final angle solution has selected the *natural* boundary condition for the maneuver. As a result, we conclude that

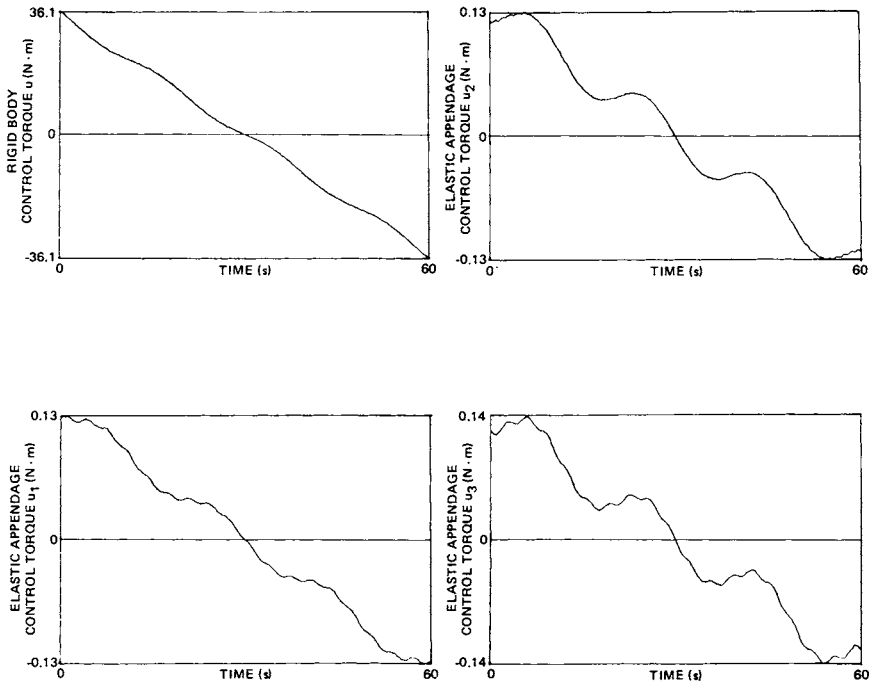

Figure 10.16 Control Torque Profiles for Case 5

Table 10.4. Summary of Results for Cases 1 Through 4

Control Derivative Index k	Peak Torque (N-m)	Peak Structural Deformations (m) 1st Mode	2nd Mode
0	38.3	2.43	0.11
1	37.2 (-2.9%)*	1.94 (20%)**	0.09 (19%)**
2	42.3 (10.0%)	2.24 (7.8%)	0.10 (9%)
3	43.7 (14%)	2.40 (1.2%)	0.10 (9%)

+k denotes the highest control time derivative

* (#%) denotes the percent change in peak torque when compared to peak torque for k = 0.

** (#%) denotes the percent change in peak modal amplitude when compared to peak modal amplitude for k = 0.

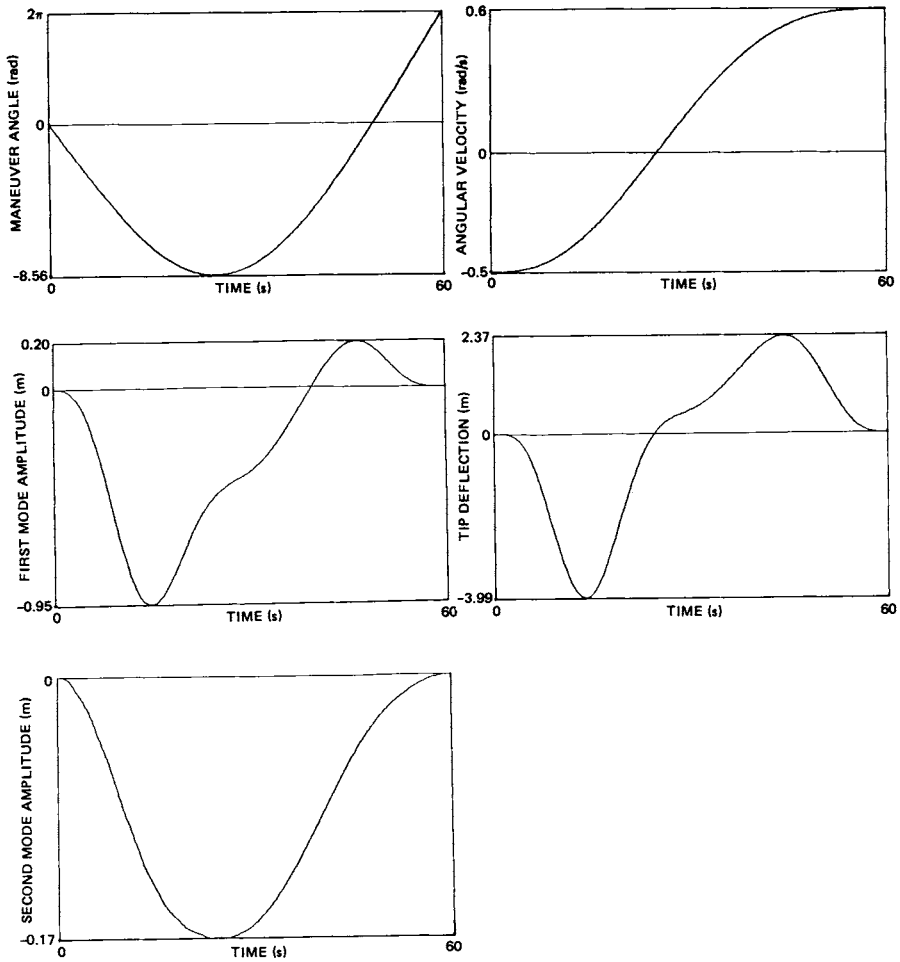

Figure 10.17 Case 6, Spin-Reversal Maneuver with Fixed Final Angle, k=2, 2 Modes, 5 Controls

for maneuvers where only the final angular rate and not the final vehicle orientation is important, the system performance is improved if free final angle solutions are used.

Case 8 (Figures 10.21 and 10.22) presents a slewing maneuver where we wish to determine the optimal stopping time for engaging and tracking a moving

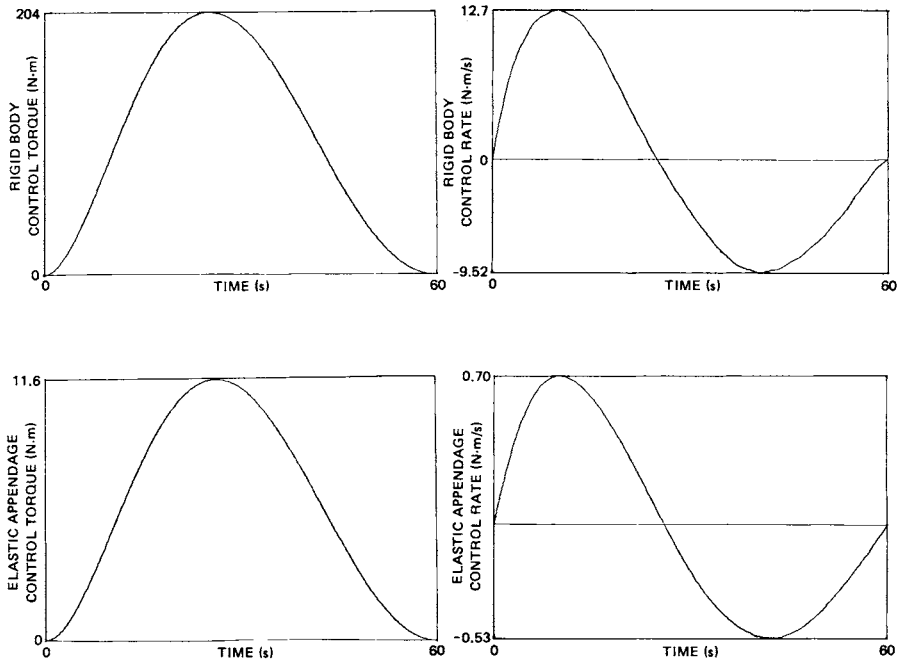

Figure 10.18 Control Torque Profiles for Case 6

target at the end of the maneuver. In this maneuver the terminal controls have not been set to zero. The formulation of Section 10.4.4 has been used for computing the optimal stopping time, t_f^*. The kinematic constraints of Table 10.2 have been rigorously satisfied, while the dynamic constraints of Table 10.2 have been approximately satisfied in a weighted least-squares sense. The position and velocity vectors for the target motion are assumed to be given by (see Fig. 10-3)

$$\mathbf{R}_T(t) = 1000\hat{\mathbf{n}}_1 + (200t - 3000)\hat{\mathbf{n}}_2$$

$$\dot{\mathbf{R}}_T(t) = 200\hat{\mathbf{n}}_2$$

$\hat{\mathbf{n}}_1, \hat{\mathbf{n}}_2$ are orthogonal inertial unit vectors, and the estimated target orientation angle, $\hat{\theta}_{target}(t)$, relative to the n-frame is

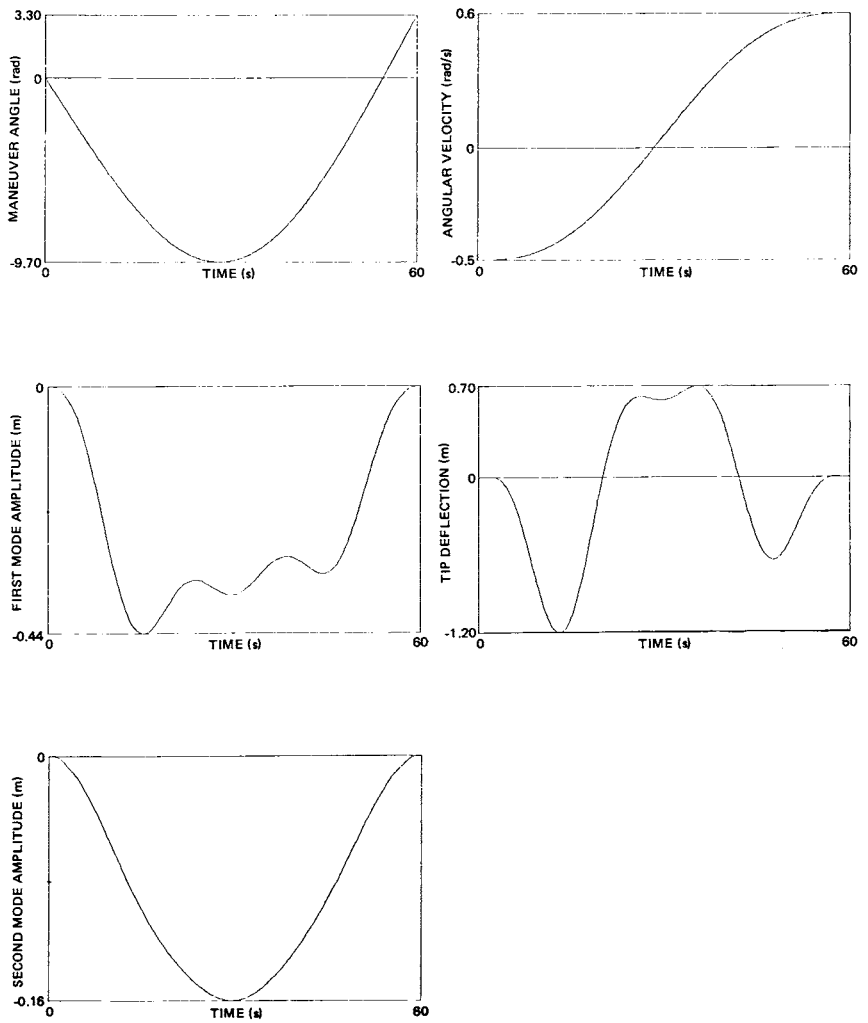

Figure 10.19 Case 7, Spin-Up Maneuvers with Free Final Angle, k=2, 2 Modes, 5 Controls

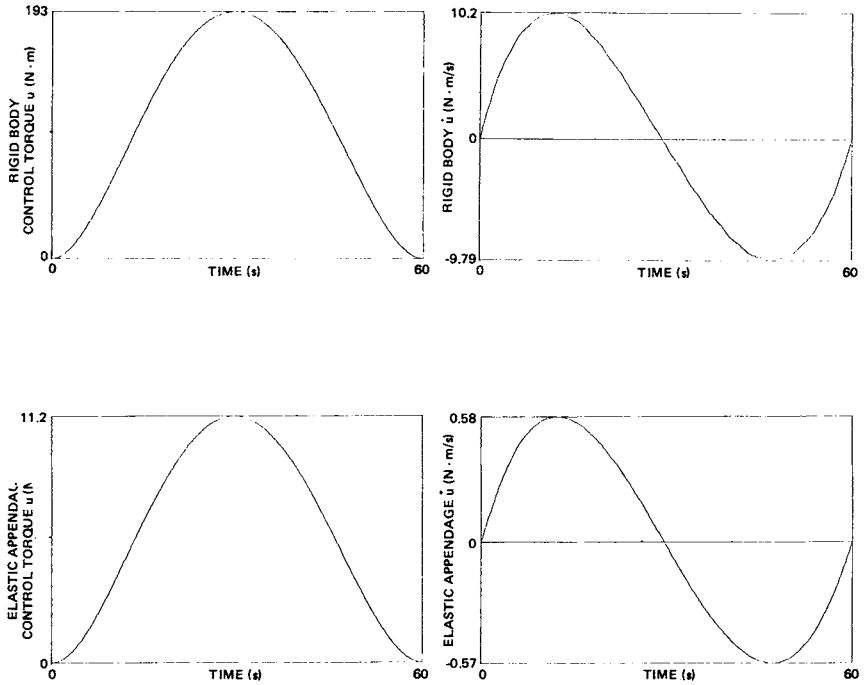

Figure 10.20 Control Torque Profiles for Case 7

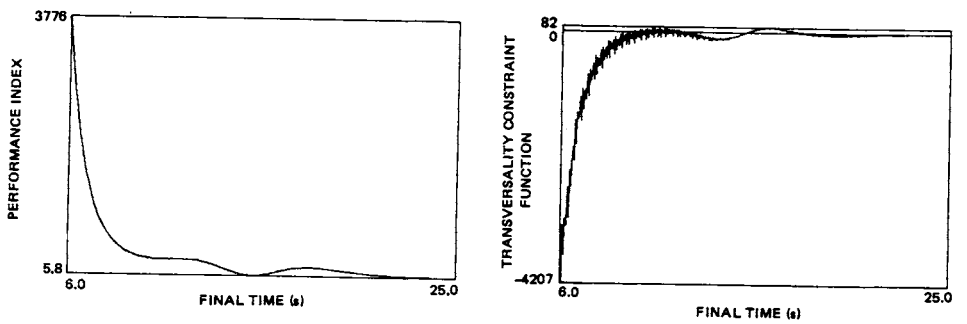

Figure 10.21 Case 8, Performance Index and Transversality Condition for an Optimal Tracking Maneuver

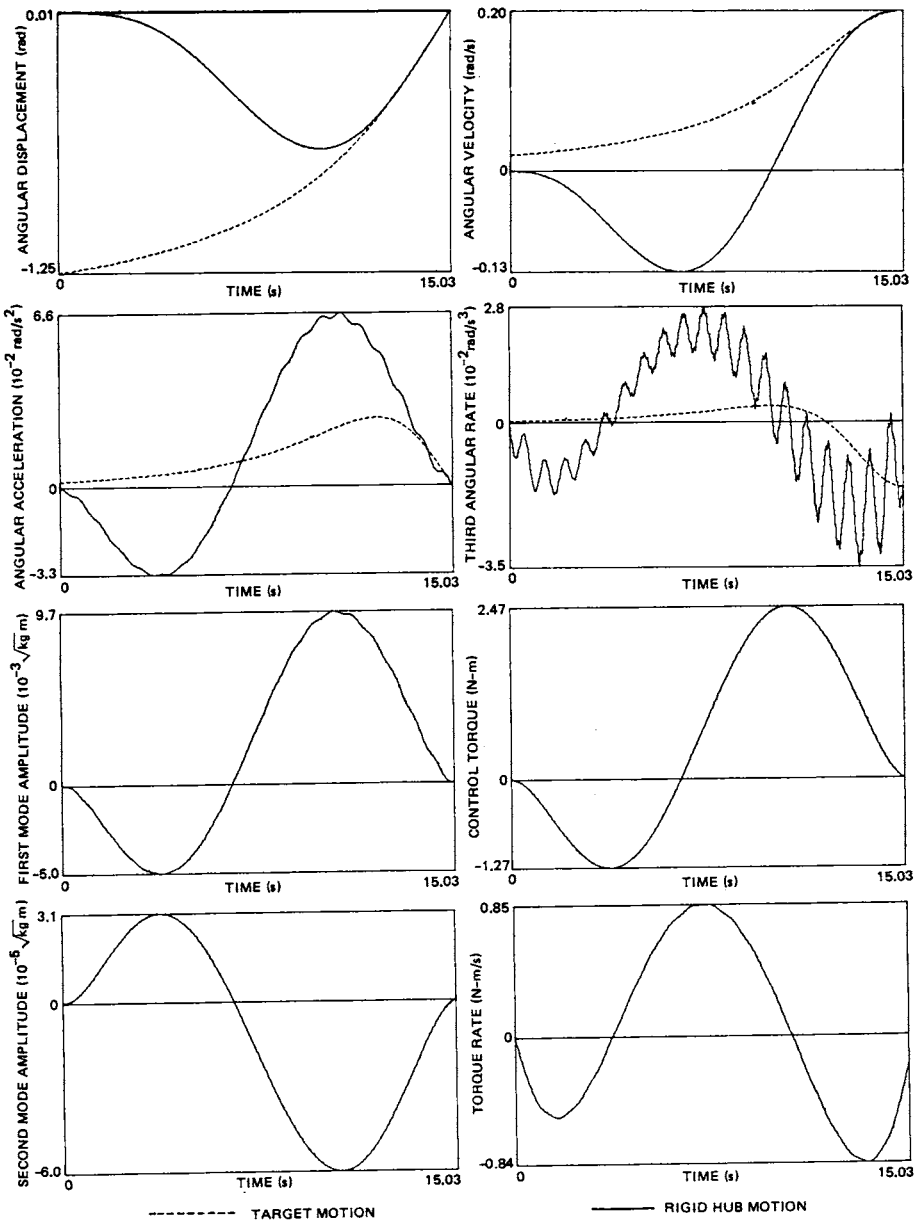

Figure 10.22 Case 8, Optimal Stopping Time Maneuver for Engaging a Moving Target, k = 2, 2 Modes

$$\hat{\theta}_{target}(t) = \tan^{-1}\left(\frac{200t-3000}{1000}\right)$$

The time derivatives of $\hat{\theta}_{target}(t_f)$ required in Eq. 10.16 are obtained by straightforward calculus from the equation above. The initial spacecraft orientation angle and angular rate are assumed to be

$$\theta(t_o) = 0 \quad , \quad \dot{\theta}(t_o) = 0$$

The initial conditions for the two flexible modal amplitudes and amplitude rates are

$$\eta(t_o) = 0 \quad , \quad \dot{\eta}(t_o) = 0 \quad (2x1)$$

The highest time derivative of the control appearing in the performance index of Eq. 10.4 is assumed to be k=2. The state, control, and pseudo-inverse weight of Eq. 10.14 are given by

$$Q = \text{Diag}(10^{-5},10^{-3},10^{-3},10^{-3},10^{-3},10^{-3},10^{-9},10^{-9})$$

$$R = 10$$

$$W = \text{Diag}(1,0,0)$$

An approximate optimal stopping time t_f was found by recursively generating the scalar value of the performance index of Eq. 10.21, and searching for the minimum value (see Fig. 10.21). From this procedure, the approximate final time was found to be $\hat{t}_f \approx 15$ sec., which is approximately the time of closest approach.

It is of interest to note in Fig. 10.21 that the performance index J has a well defined local minimum near $\hat{t}_f$. However, the transversality constraint function of Eq. 10.17 has many local minima. Nevertheless, the transversality constraint function is well behaved in the vincinity of the local minimum of the performance index. This problem highlights the potential difficulties one can encounter by solely relying on the transversality conditions for insight into the optimal solution. Indeed, if the analyst had selected starting guesses for t_f more than a few seconds from the solution, the converged local

solution would most likely be guess-dependent. After iterative refinement, the converged solution is found to be $t_f^* = 15.03213$ sec. From Fig. 10.22 it follows that the vehicle reverses the algebraic sign of its angular velocity twice. First, to backup relative to the direction of the target motion. Second, to spin reverse in order to catch the target at t_f^*. From Fig. 10.22 the vehicle and target motion are seen to osculate at the final time for several time derivatives. Moreover, the attitude motion of the vehicle and target are seen to overlap to plotting accuracy for approximately one fifth of the maneuver.

10.6 CONCLUDING REMARKS

From the results of Section 10.6, we can reach the following conclusions about the control-rate penalty method:

(1) The terminal jump discontinuities in the control-time histories have been moved into the higher control time derivatives.

(2) As shown in the Fourier transforms of the controls, the frequency content of the "smoothed" control has been significantly reduced when compared to the k=0 maneuver profile (i.e., a k+1 pole roll-off). Accordingly, the higher frequency modes are only mildly excited during the various maneuvers.

(3) The use of smoothed control profiles yields a greater gain in system performance than spatially distributing the discrete control actuators. However, by combining both smoothed control and multiple actuators, further gains in the system performance can be realized.

(4) As shown in the free final angle maneuver of Case 7, the system response is improved if we formulate the problem in such a way that the control algorithm selects the *natural* boundary condition for the maneuver.

(5) The use of control-rate penalties significantly reduces the structural deformations during large-angle rotational maneuvers.

(6) As shown in optimal stopping time maneuver of Case 8, the design freedom available to the analyst by using control-rate penalties, can be exploited for satisfying a variety of physically meaningful boundary conditions.

REFERENCES

1. Lassen, H. A. and Elliot, L. E., "Use of Control of Higher Order Derivatives of Excitation to Minimize Dynamic Response," TRW IOC, January 7, 1977.

2. Farrenkopf, R. L., "Optimal Open-Loop Maneuver Profiles for Flexible Spacecraft," Paper No. 78-1280, Presented at the AIAA Guidance and Control Conference, Palo Alto, California, August 1978.

3. Swigert, C. J., "Shaped Torques Technique," Paper No. 78-1692, presented at the AIAA Conference on Large Space Platforms: Future Needs and Capabilities, Los Angeles, California, September 1978.

4. Turner, J. D. and Chun, H. M., "Optimal Distributed Control of a Flexible Spacecraft Using Control-Rate Penalties in the Controller Design," Paper No. 82-1438, presented at the AIAA Astrodynamics Conference, San Diego, California, August 9-11, 1982.

5. Junkins, J. L., "Comment on Optimal Feedback Slewing of Flexible Spacecraft," **Journal of Guidance, Control, and Dynamics**, Vol. 5, No. 3, May-June 1982, p. 318.

6. Turner, J. D., Chun, H. M., and Juang, J-N., "Closed-Form Solutions for a Class of Optimal Quadratic Tracking Problems," **Journal of Optimization Theory and Applications**, (to appear).

7. Juang, J-N., Turner, J. D., and Chun, H. M., "Closed-Form Solutions for Feedback Control with Terminal Constraints," **Journal of Guidance, Control, and Dynamics**, Vol. 8, No. 1, Jan.-Feb., 1985, pp. 39-43.

8. Juang, J-N., Turner, J. D., and Chun, H. M., "Closed-Form Solutions for a Class of Optimal Quadratic Tracking Problems with Terminal Constraints," **Journal of Dynamic Systems, Measurement and Control**, (to appear).

9. Chun, H. M., Turner, J. D., and Juang, J-N., "Disturbance-Accommodating Tracking Maneuvers of Flexible Spacecraft," **The Journal of the Astronautical Sciences**, Vol. 33, No. 2, April-June, 1985, pp. 197-216.

10. Aspinwall, D. W., "Acceleration Profiles for Minimizing Residual Response," **Journal of Dynamic Systems, Measurement, and Control**, Vol. 102, March 1980.

11. Gupta, N. K., "Frequency Shaping of Cost Functionals: An Extension of Linear-Quadratic-Gaussian Design Methods," **Journal of Guidance and Control**, Vol. 3, No. 6, November-December 1980, pp. 529-535.

12. Gupta, N. K., "Robust Control/Estimator Design by Frequency Shaped Cost Functionals," presented at the 20th Decision and Control Conference, San Diego, California, 1981.

13. Aubrun, J., Breakwell, J., Gupta, N., Lyons, M., and Margulies, G., "ACOSS FIVE (Active Control of Space Structures) Phase IA," RADC-TR-82-21, March 1982.

14. Skaar, S. B. and Tucker, D., "The Optimal Control of Flexible Systems Using a Convolution Integral Description of Motion," Proceedings of the 22nd IEEE Conference on Decision and Control, San Antonio, Texas, December 14-16, 1983.

15. Moore, J. B., and Anderson, B. D. O., "Optimal Linear Control Systems with Input Derivative Constraints," Proc. IEEE, Vol. 114, No. 12, 1967, pp. 1987-1990.

16. Chun, H. M., "Optimal Distributed Control of a Flexible Spacecraft During a Large-Angle Maneuver," MS Thesis, MIT, Cambridge, Massachusetts, 1982.

17. Turner, J. D., Chun, H. M., et al., "ACOSS Eleven Semiannual Technical Report," CSDL-R-1536, Contract No. F30602-81-C-0180, The Charles Stark Draper Laboratory, Inc., February 1982.

18. Van Loan, C. F., "Computing Integrals Involving the Matrix Exponential," **IEEE Transactions on Automatic Control**, Vol AC-23, No. 3, June 1978.